



## Novel inhibitors of leukocyte transendothelial migration

Tamar Getter<sup>a,1</sup>, Raanan Margalit<sup>b,e</sup>, Shirin Kahremany<sup>a,1</sup>, Laura Levy<sup>a</sup>, Eliav Blum<sup>a</sup>, Netaly Khazanov<sup>a</sup>, Nimrod Y. Keshet-Levy<sup>a,c</sup>, Tigist Y. Tamir<sup>d</sup>, M. Ben Major<sup>d</sup>, Ron Lahav<sup>e</sup>, Sofia Zilber<sup>c</sup>, Hanoch Senderowitz<sup>a</sup>, Paul Bradfield<sup>f</sup>, Beat A. Imhof<sup>g</sup>, Evgenia Alpert<sup>e,\*</sup>, Arie Gruzman<sup>a,\*</sup>

<sup>a</sup> Division of Medicinal Chemistry, Department of Chemistry, Faculty of Exact Sciences, Bar-Ilan University, Ramat-Gan, Israel

<sup>b</sup> "Science in Action", Ness-Ziona, Israel

<sup>c</sup> Department of Pathology, Shaare Zedek Medical Center, Jerusalem, Israel

<sup>d</sup> Department of Pharmacology and the Lineberger Comprehensive Cancer Center, University of North Carolina at Chapel Hill, Chapel Hill, NC 27599, USA

<sup>e</sup> "Alta-Zuz Therapeutics", Ness-Ziona, Israel

<sup>f</sup> "MesenFlow Technologies", Geneva, Switzerland

<sup>g</sup> Department of Pathology and Immunology, University of Geneva, Geneva, Switzerland

### ARTICLE INFO

#### Keywords:

Leukocyte transmigration  
 Trioxotetrahydropyrimidin derivatives  
 Multiple sclerosis  
 IBD/Crohn's disease  
 Arthritis  
 Fatty liver

### ABSTRACT

Leukocyte transendothelial migration is one of the most important step in launching an inflammatory immune response and chronic inflammation can lead to devastating diseases. Leukocyte migration inhibitors are considered as promising and potentially effective therapeutic agents to treat inflammatory and auto-immune disorders. In this study, based on previous trioxotetrahydropyrimidin based integrin inhibitors that suboptimally blocked leukocyte adhesion, twelve molecules with a modified scaffold were designed, synthesized, and tested *in vitro* for their capacity to block the transendothelial migration of immune cells. One of the molecules, namely, methyl 4-((2-(*tert*-butyl)-6-((2,4,6-trioxotetrahydropyrimidin-5(2H)-ylidene) methyl) phenoxy) methyl) benzoate, (compound **12**), completely blocked leukocyte transendothelial migration, without any toxic effects on immune or endothelial cells ( $IC_{50} = 2.4 \mu M$ ). *In vivo*, compound **12** exhibited significant therapeutic effects in inflammatory bowel disease (IBD)/Crohn's disease, multiple sclerosis, fatty liver disease, and rheumatoid arthritis models. A detailed acute and chronic toxicity profile of the lead compound *in vivo* did not reveal any toxic effects. Such a type of molecule might therefore provide a unique starting point for designing a novel class of leukocyte transmigration blocking agents with broad therapeutic applications in inflammatory and auto-immune pathologies.

**Abbreviations:** ANOVA, analysis of variance; AUC, area under the curve; CII, type II collagen; CNS, central nervous system; CXCL, chemokine (C-X-C motif) ligand; CIA, collagen-induced arthritis; CFA, complete Freund's adjuvant; CD, chow diet; CRN, clinical research network; DDW, double distilled water; DAI, disease activity index; DMEM, Dulbecco's modified Eagle medium; DMF, dimethylformamide; DMSO, dimethyl sulfoxide; DSS, dextran sulfate sodium salt; EAE, experimental autoimmune encephalomyelitis; ECs, endothelial cells; ESI, electrospray ionization; FCS, fetal calf serum; FLIP, fatty liver inhibition of progression;  $F^{19}$ -NMR, Fluorine-19 nuclear magnetic resonance spectroscopy; GLP, good laboratory practice; H&E, hematoxylin and eosin; HPLC, high-performance liquid chromatography; HUVEC, human umbilical vein endothelial cells; HRMS, high-resolution mass spectra; IBD, inflammatory bowel disease; Interferon  $\gamma$  (IFN $\gamma$ ); IP, intraperitoneal; IFD, induced fit docking; IV, intravenous; JAM-C, junction adhesion molecule 1; KO, knockout; LBRC, lateral border recycling compartment; LDT, leucine-aspartic acid-threonine; MAdCAM-1, mucosal vascular addressin cell adhesion molecule 1; MOG, myelin oligodendrocyte glycoprotein; NW, normal water; NAFLD, non-alcoholic fatty liver dystrophy; NAS, NAFLD activity score; PECAM-1, platelet endothelial cell adhesion molecule 1; RPMI, Roswell park memorial institute; PPAR- $\gamma$ , peroxisome proliferator-activated receptor; PO, per os (oral administration); PTX, pertussis toxin; PBS, phosphate buffer solution; RIPA, radioimmunoprecipitation assay buffer; ROC, receiver operating characteristic; SC, sub-cutaneous; SEM, standard error measurements; THF, tetrahydrofuran; TLC, thin-layer chromatography; TMS, tetramethylsilane TNF- $\alpha$ , tumor necrosis factor  $\alpha$ ; VCAM-1, vascular cell adhesion protein 1; WD, western diet

\* Corresponding authors.

E-mail addresses: [genia.a@ayalapharma.com](mailto:genia.a@ayalapharma.com) (E. Alpert), [gruzmaa@biu.ac.il](mailto:gruzmaa@biu.ac.il) (A. Gruzman).

<sup>1</sup> Present addresses: Department of Ophthalmology, Gavin Herbert Eye Institute, UCI Health, Orange County, CA, USA.

<https://doi.org/10.1016/j.bioorg.2019.103250>

Received 30 May 2019; Received in revised form 2 September 2019; Accepted 3 September 2019

Available online 09 September 2019

0045-2068/ © 2019 Elsevier Inc. All rights reserved.

## 1. Introduction

Inflammatory and autoimmune diseases represent a significant proportion of devastating human pathologies [1–4]. Dozens of drugs are currently in use to treat these disorders [5–7]. However, often complete remission is not achieved and most of the drugs have serious side effects [8,9]. Several autoimmune and chronic inflammatory diseases, such as Crohn's disease, multiple sclerosis, ankylosing spondylitis, psoriasis, rheumatoid arthritis, or lupus erythematosus and many others are not treatable or have poor treatment response and are often fatal [10,11].

Thus, the discovery and design of novel drugs against inflammatory and autoimmune diseases is one of the major directions in the pharmaceutical industry and in academia. For example, there were around 400 ongoing clinical trials for treating rheumatoid arthritis in 2018 alone. <https://www.centerwatch.com/clinical-trials/listings/therapeutic-area/19/rheumatology/>.

Therefore, the molecular processes that define and regulate the recruitment of leukocytes as part of inflammation have been identified as potential targets in drug development since the 1990s [12–14]. Historically, integrins have been the focus of drug development and their inhibition was generated by monoclonal antibodies, peptides/peptidomimetics, and small organic molecules [15]. Several integrin antagonists or modulators of their binding ligands have exhibited clinically significant benefits, leading to continued medical interest in further development of novel integrin inhibitors [16]. Currently, almost all human integrins have been used as a target for developing effective antagonists [14].

Integrin  $\alpha 4 \beta 7$  plays an important role in the leukocyte transmigration process [15]. One of the most important binding partners of integrin  $\alpha 4 \beta 7$  is mucosal vascular addressin cell adhesion molecule 1 (MAdCAM-1) [17]. This protein is predominantly expressed in the mesenteric lymph nodes and Peyer's patches [18,19]. However, under inflammatory stimuli, the expression level of MAdCAM-1 in vascular endothelial cells is upregulated [20]. The protein translocated to the plasma membrane and leads to augmented adhesion of  $\alpha 4 \beta 7$  integrin-positive lymphocytes to the endothelium [21]. In particular, the interaction between  $\alpha 4 \beta 7$  and MAdCAM-1 is considered to be one of the most vital events in regulating leukocyte trafficking in the gastrointestinal tract [22,23]. It is therefore not surprising that both proteins have been shown to be involved in the pathophysiology of inflammatory bowel diseases (IBD) [24], and they have been targeted by several drugs, for example, by vedolizumab, a humanized monoclonal antibody that recognizes the gut-specific  $\alpha 4 \beta 7$  integrin [25,26].

In addition to biological drugs, small-molecule inhibitors of that interaction were also developed. In 1996 Fong's group at Genentech showed that MAdCAM-1 binds to  $\alpha 4 \beta 7$  integrin via the specific amino acid sequence leucine–aspartic acid–threonine (LDT) motif [27]. Since then, several mimicking LDT moiety inhibitors have been developed [28,29]. In addition, some very potent MAdCAM-1 and  $\alpha 4 \beta 7$  integrin interaction blockers have been developed without targeting the LDT sequence [30–32]. In 2008, Briskin's group at Millenium Pharmaceuticals published a paper in which they described the discovery of a trioxotetrahydropyrimidin-based antagonist that specifically blocks the  $\alpha 4 \beta 7$  integrin MAdCAM-1 interaction, without indicating that this inhibition was mediated by the LDT sequence. All compounds reported by the group were selected via high-throughput screening results based on the static whole-cell adhesion assay [33]. In addition, several other trioxotetrahydropyrimidin derivatives were reported as anti-inflammatory agents [34].

Here we describe the design, synthesis, and biological evaluation of twelve trioxotetrahydropyrimidin derivatives that significantly differed in structure from the set of compounds previously described by the group of M. Briskin. The lead compound, methyl 4-((2-*tert*-butyl)-6-((2,4,6-trioxotetrahydropyrimidin-5(2H)-ylidene) methyl) phenoxy) methyl) benzoate (12), completely inhibited monocyte, T lymphocytes,

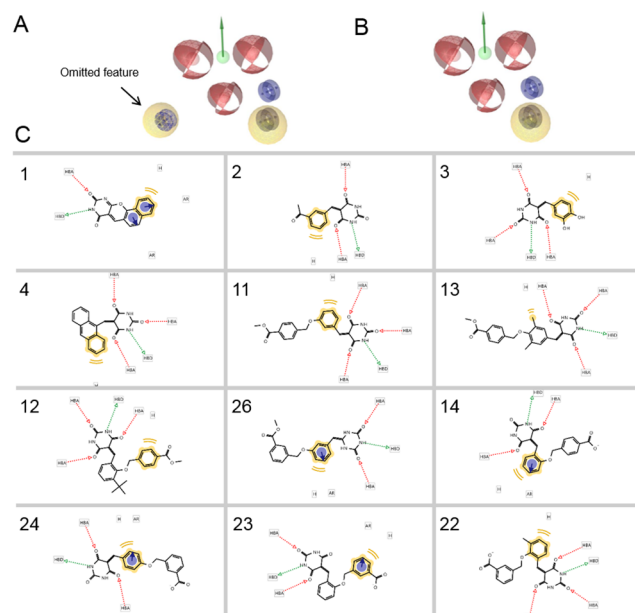


**Fig. 1.** Ligand-based pharmacophore model developed using the LigandScout program. (A) A pharmacophore model design based on the trioxotetrahydropyrimidin derivative structures described by Harriman et al. (B) The pharmacophore model includes two aromatic rings (blue)- AR, one hydrophobic (yellow)- H, three hydrogen acceptor features (red)- HBA, and one hydrogen donor (green)- HBD. (C) A pharmacophore mapped 2D feature representation of the designed compounds. The features are color-coded, as described above.

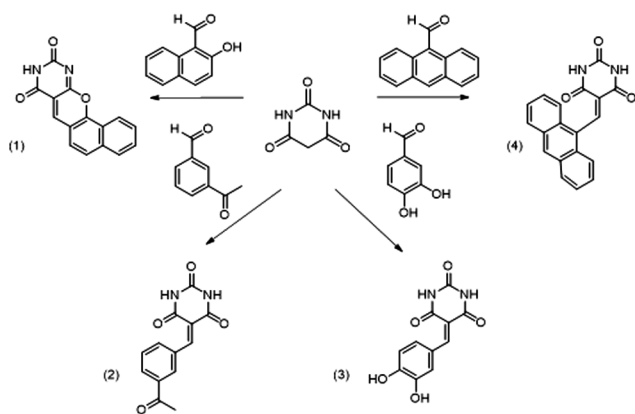
and B lymphocyte transendothelial migration *in vitro*. A significant *in vivo* effect of compound 12 was also observed in multiple sclerosis, arthritis, fatty liver, and in IBD mouse models. Compound 12 did not display any toxic effects in mice in concentrations up to 200 mg/kg, at multi-dose administration during a 28-day period. Surprisingly, compound 12 did not block MAdCAM-1 as we had previously anticipated. Based on *in silico* calculation, we now hypothesize that compound 12 instead may block platelet endothelial cell adhesion molecule 1 (PECAM-1) based transendothelial migration of leukocytes. Such types of molecules might therefore provide a unique starting point for designing a novel class of leukocyte transmigration blocking agents with broad therapeutic applications.

## 2. Results and discussion

### 2.1. Chemistry

Based on the trioxotetrahydropyrimidin derivative structures, described by Harriman et al. [33] (Supporting Information Chart 1), we designed a ligand-based pharmacophore model using the LigandScout platform (Fig. 1A) [35,36]. The resulting pharmacophore model contained three hydrogen acceptor features, which represented the oxygen of the carbonyl moieties, one hydrogen donor representing the amine donor, aromatic rings, and two merged hydrophobic aromatic features, representing the aromatic substitution rings in the structures of all trioxotetrahydropyrimidin derivatives. In order to simplify the structures of the designed compounds and to avoid the formation of *cis* and *trans* isomers by substituting the amide moiety of trioxotetrahydropyrimidin (similarly to all compounds that were developed by Harriman et al.), we decided to omit one of the merged pharmacophore features that represent the substitution of the amide moiety of trioxotetrahydropyrimidin.

The pharmacophore (Fig. 1B), which was changed accordingly, was used for aligning the designed compounds 1–4, 11–14, 26, and 22–24, and for evaluating their suitability for the pharmacophore (Fig. 1C). By



**Scheme 1.** Synthesis of four benzylidene pyrimidine derivative compounds 1–4: EtOH:H<sub>2</sub>O 1:1, barbituric acid, under reflux overnight.

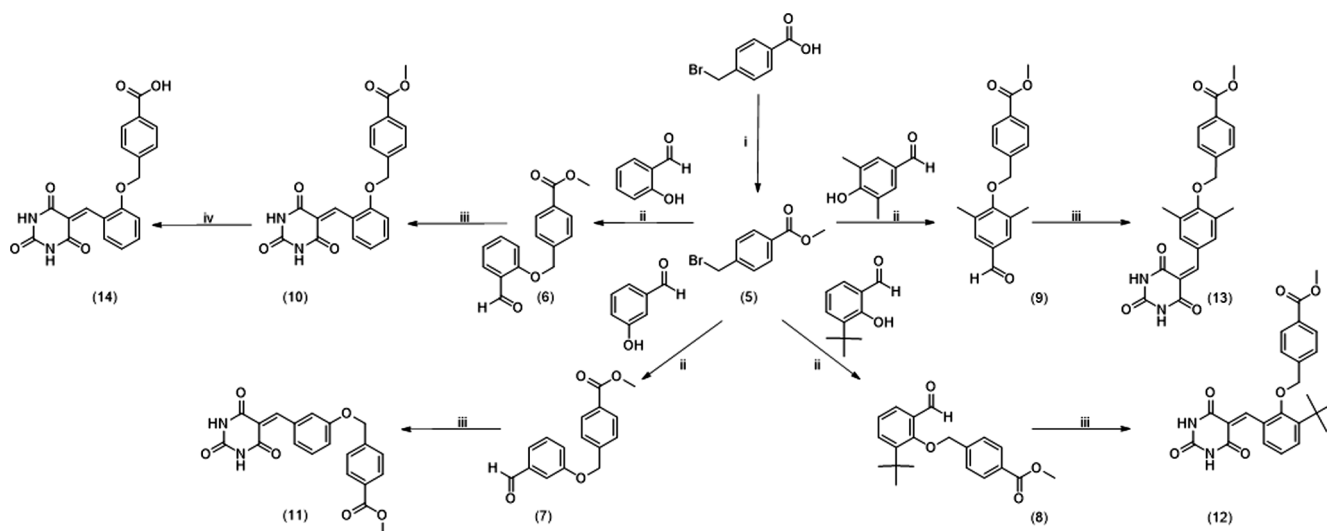
performing this step, we developed compounds with the potential to block leukocyte transmigration process.

First, four trioxotetrahydropyrimidin derivatives were synthesized, as shown in [Scheme 1](#), using classical Knoevenagel condensation between acidic hydrogens located between two carbonyls of trioxotetrahydropyrimidin and the corresponding aromatic aldehydes. Usually, a weak basic amine is used to catalyze such a reaction; however, the high acidic properties of a trioxotetrahydropyrimidin lead to deprotonation without the addition of a basic catalyst. First, four trioxotetrahydropyrimidin derivatives were obtained: 8*H*-benzo[7,8]chromeno[2,3-*d*]pyrimidine-8,10(9*H*)-dione, (1) 5-(3-acetylbenzylidene)pyrimidine-2,4,6(1*H*,3*H*,5*H*)-trione, (2) 5-(3,4-dihydroxybenzylidene)pyrimidine-2,4,6(1*H*,3*H*,5*H*)-trione, (3) 5-(anthracen-9-ylmethylene)pyrimidine-2,4,6(1*H*,3*H*,5*H*)-trione, and (4) using known synthetic procedures [37,38].

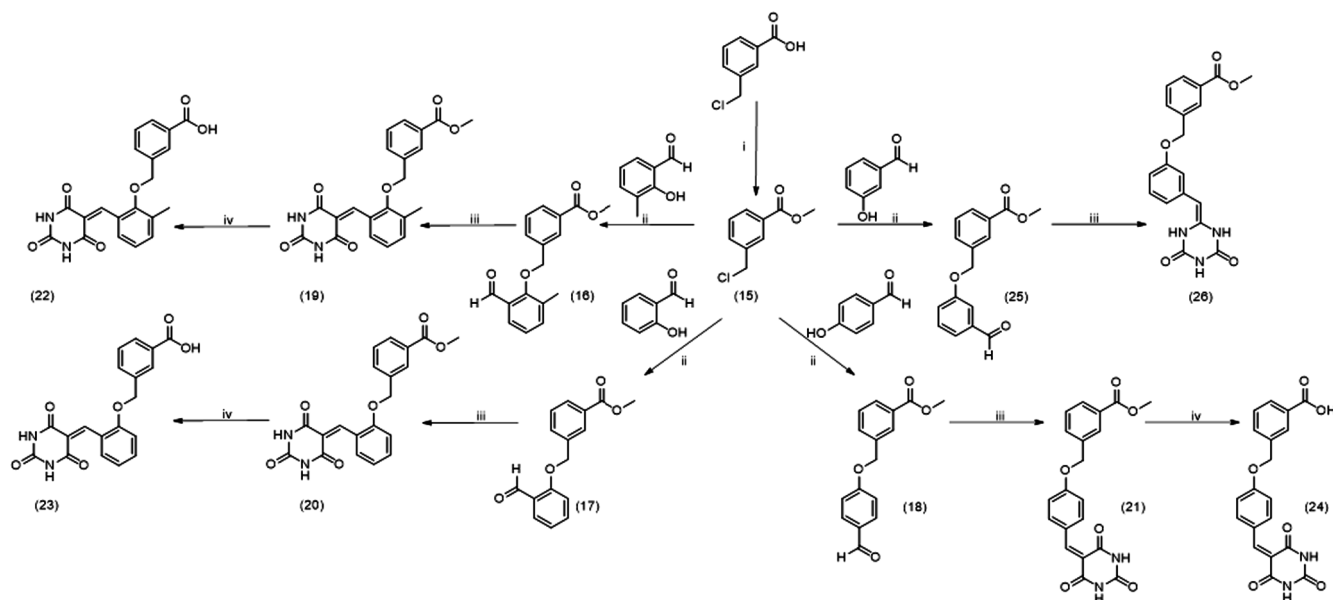
The structures of compounds 3 and 4 were already reported in the scientific literature [39,40]. However, compounds 1 and 2 are novel. It is important to mention that compound 1 was obtained unexpectedly. We planned to synthesize a molecule with a free hydroxyl group on the *ortho* to the aldehyde position. However, as a result of an intramolecular reaction, the formation of a 3,6-dihydro-2*H*-pyran derivative was observed. We presume that the driving force for the cyclization was the formation of a stable six-member ring with conjugated double bonds. As a result, only an O-cyclic compound was obtained with high yield (around 95%) and no compound with free hydroxyl.

The synthesis procedure for more complex novel trioxotetrahydropyrimidin derivatives is presented in [Scheme 2](#). Using another classical organic synthesis method, Fischer-Speier esterification, a 4-bromo-methylbenzoic acid was refluxed with methyl alcohol in the presence of a catalytic amount of H<sub>2</sub>SO<sub>4</sub> to obtain the corresponding ester: methyl 4-(bromomethyl) benzoate, (5) [41]. This was followed by reaction of 5 with commercially available hydroxybenzaldehydes, using the procedure described by Zidar et al. [42]. In which the bromine moiety changes *in situ* with a better leaving group (iodine) and by using a weak basic compound (potassium carbonate) to deprotonate the phenol moiety to couple with iodobenzyl to obtain the corresponding ether. The resulting substituted aldehydes; methyl 4-((2-formylphenoxy) methyl) benzoate (6), methyl 4-((3-formylphenoxy) methyl) benzoate (7), methyl 4-((2-*tert*-butyl-6-formylphenoxy) methyl) benzoate (8), and methyl 4-((4-formyl-2,6-dimethylphenoxy) methyl) benzoate (9) were coupled with barbituric acid using Knoevenagel condensation (without the addition of a basic catalyst) to obtain methyl 4-((2-((2,4,6-trioxotetrahydropyrimidin-5(2*H*)-ylidene) methyl) phenoxy) methyl) benzoate (10), methyl 4-((3-((2,4,6-trioxotetrahydropyrimidin-5(2*H*)-ylidene) methyl) phenoxy) methyl) benzoate (11), methyl 4-((2-((*tert*-butyl)-6-((2,4,6-trioxotetrahydropyrimidin-5(2*H*)-ylidene) methyl) phenoxy) methyl) benzoate (12), and methyl 4-((2,6-dimethyl-4-((2,4,6-trioxotetrahydropyrimidin-5(2*H*)-ylidene) methyl) phenoxy) methyl) benzoate (13), respectively. Compound 4-((2-((2,4,6-trioxotetrahydropyrimidin-5(2*H*)-ylidene) methyl) phenoxy) methyl) benzoic acid (14) was obtained using strong basic catalysis of a hydrolysis of the ester bond in the presence of sodium hydroxide. Following an almost identical synthetic pathway, but using as a starting material a 3-(chloromethyl)-benzoic acid, an additional set of novel trioxotetrahydropyrimidin derivatives were synthesized, as shown in [Scheme 3](#). This set consists of methyl 3-((2-methyl-6-((2,4,6-trioxotetrahydropyrimidin-5(2*H*)-ylidene) methyl) phenoxy) methyl) benzoate (19), methyl 3-((2-((2,4,6-trioxotetrahydropyrimidin-5(2*H*)-ylidene) methyl) phenoxy) methyl) benzoate (20), methyl 3-((4-((2,4,6-trioxotetrahydropyrimidin-5(2*H*)-ylidene) methyl) phenoxy) methyl) benzoate (21), 3-((2-methyl-6-((2,4,6-trioxotetrahydropyrimidin-5(2*H*)-ylidene) methyl) phenoxy) methyl) benzoic acid (22), 3-((2-((2,4,6-trioxotetrahydropyrimidin-5(2*H*)-ylidene) methyl) phenoxy) methyl) benzoic acid (23), 3-((4-((2,4,6-trioxotetrahydropyrimidin-5(2*H*)-ylidene) methyl) phenoxy) methyl) benzoic acid (24), and methyl 3-((3-((4,6-dioxo-1,3,5-triazinan-2-ylidene) methyl) phenoxy) methyl) benzoate (26).

In [Scheme 4](#) shown the synthetic pathway for the preparation of <sup>19</sup>F labeled derivative of compound 12 which was obtained as described in



**Scheme 2.** Synthetic pathways of four benzylidene pyrimidine derivative compounds 11–14: (i) MeOH, H<sub>2</sub>SO<sub>4</sub>, under reflux for 5 h. (ii) K<sub>2</sub>CO<sub>3</sub>, KI, salicylaldehyde, CH<sub>3</sub>CN, 70 °C for 5 h. (iii) EtOH/H<sub>2</sub>O 1:1, barbituric acid, under reflux overnight. (iv) 2 M NaOH, 1,4 dioxan:MeOH:H<sub>2</sub>O 1:1:1, under reflux for 5 h.



**Scheme 3.** Synthetic pathways of four benzylidene pyrimidine derivative compounds **22–24** and **26**: (i) MeOH, H<sub>2</sub>SO<sub>4</sub>, under reflux for 5 h. (ii) K<sub>2</sub>CO<sub>3</sub>, KI, CH<sub>3</sub>CN, 70 °C for 5 h. (iii) EtOH/H<sub>2</sub>O 1:1, barbituric acid, reflux overnight. (iv) 2 M NaOH, 1,4 dioxan:MeOH:H<sub>2</sub>O 1:1:1, under reflux for 5 h.

**Scheme 1.** Compound **30** was used for the determination of the level of HeLa cell labeling by <sup>19</sup>F NMR.

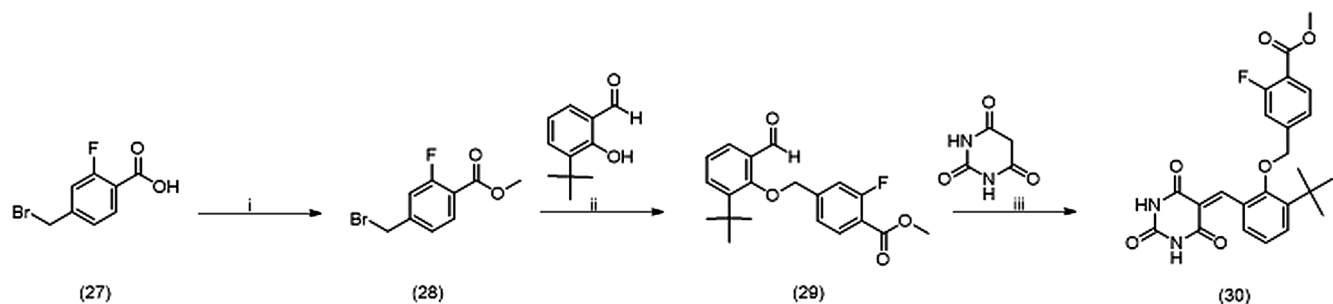
## 2.2. *In vitro* study of the anti-inflammatory effects

The synthesized compounds were evaluated *in vitro* using a bio-imaging platform that provides a detailed analysis of individual leukocyte interactions with vascular endothelial cells (ECs) under physiological flow that occurs during inflammatory reactions [43]. This technique allowed us to determine the possible effects of compounds on four major mechanisms that define human leukocyte trafficking using primary cells: (1) the initial capture of leukocytes in free-flow onto endothelial luminal surfaces, which is rapidly followed by (2) firm adhesion, and (3) the migration of monocytes on the endothelial surface (pre-transmigration event). Luminal movement can then lead to migration of the leukocyte across the endothelial barrier into the abluminal compartment, termed leukocyte trans-endothelial migration (between EC junctions) area, followed by (4) migration into the abluminal extracellular matrix or eventually, reverse transmigration back into the vascular lumen.

The underlying trafficking mechanisms of human monocytes were investigated using a flow assay bio-imaging system in the presence of the tested compounds [44]. A monolayer of human umbilical vein endothelial cells (HUVECs) was cultured in flow chambers that allowed human monocytes, T- or B- lymphocytes to be perfused over the endothelial monolayer under physiological shear stress conditions

representing capillary flow rates *in vivo* (Supporting Information Fig. S1). Using phase contrast bio-imaging, we were able to film (Movie 1) the perfused leukocytes undergoing capture, their firm adhesion to endothelial cells, followed by transendothelial migration and thus determine how this process may be affected by the tested compounds. A summary of the results is presented in Fig. 2. Briefly, a monocyte suspension was flowed over tumor necrosis factor  $\alpha$  (TNF- $\alpha$ ) activated HUVECs for the first 5 min of the experiment, before switching to the wash buffer for 40 min. The adherent monocytes appeared as phase-white, which rapidly changed to phase-gray as the cells became firmly adherent. Monocytes that transmigrated through the HUVEC monolayer changed from a phase-gray to a phase-black appearance. This change in the cells' appearance and the phases in migration enabled us to measure every aspect of monocyte recruitment. Under control conditions, the captured monocytes became adherent within 1 min, and transmigrated within 15 min of flow co-culture. Four compounds: **4**, **11**, **12**, and **26** displayed a significant inhibitory effect in this screening system.

Another parameter that was measured in the monocyte transmigration assay is the level of adhesion of monocytes to the endothelial cells. This parameter was used to determine whether the inhibitory effects of active compounds are related to their intervention with adhesion or to the transmigration pathway itself. The effect of the most active compounds **4**, **12**, and **26** on the adhesion of monocytes was tested. We dropped in this stage compound **11**, because it was less active than **12** and **26** but its activity was similar to **4**. The adhesion was



**Scheme 4.** Synthetic pathways of fluorinated benzylidene pyrimidine derivative compound **30**: (i) MeOH, H<sub>2</sub>SO<sub>4</sub>, under reflux for 5 h. (ii) K<sub>2</sub>CO<sub>3</sub>, KI, salicylaldehyde, CH<sub>3</sub>CN, 70 °C for 5 h. (iii) EtOH/H<sub>2</sub>O 1:1, barbituric acid, under reflux overnight. Compound **28** is a known molecule.

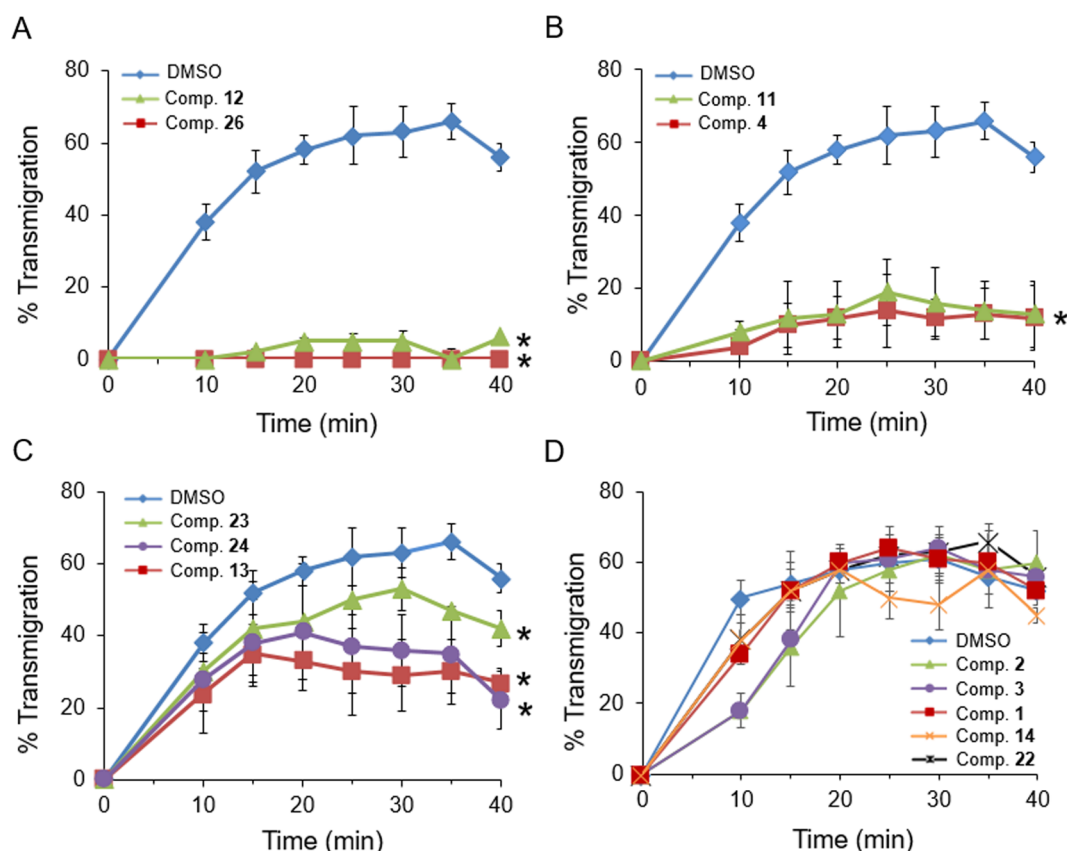


Fig. 2. Monocyte transmigration on the surface of activated HUVECs under flow. Primary human monocytes co-cultured on TNF- $\alpha$ -activated HUVECs. Test compounds at 30  $\mu$ M or DMSO (blue line) were added to cells for 45 min. Co-cultures were kept under a flow of 0.05 Pa. (A) Compounds 12 (red line) and 26 (green line). Total blocking of transmigration. (B) Compounds 4 (red line) and 11 (green line). High levels of blocking. (C) Compounds 13 (red line), 23 (green line), and 24 (purple line). Low levels of blocking. (D) Compounds 1 (red line), 2 (green line), 3 (purple line), 14 (orange line), and 22 (black line). No effect.  $n = 3$ . Mean  $\pm$  SE, \* $P \leq 0.05$ .

found to be unaffected for all three tested compounds (Fig. 3A). The effect on the transmigration process was then determined again for all three molecules (Fig. 3B).

Two compounds, 12 and 26, exhibited a very effective inhibition of monocyte transmigration. However, compound 12 completely blocked monocyte transmigration at a 30  $\mu$ M concentration, and not even a single blocked monocyte undergoing transmigration could be recorded (Movie 1).

In general, from the most active compound, 12, several conclusions of the structure-activity relationship results could be drawn. For example, compound 4 has an anthracene moiety instead of the di-aromatic-substituted one in compounds 12 and 26. This compound exhibited an inhibitory effect similar to compounds 26 and 12 but with less potency. This means that bulky substitution for trioxotetrahydropyrimidin might be critical for achieving high-efficacy compounds. Compound 26 is similar to the most potent and active compound 12. However, the absence of *t*-butyl substitution and the *meta* position of the benzyl ether instead of the *ortho* one in compound 12 decreased dramatically the activity of compound 26. Consequently, we propose that the *t*-butyl moiety might be critical for binding to a hydrophobic pocket of target protein. Compound 11 has no *t*-butyl substitution and the trioxotetrahydropyrimidin groups are located at the *meta* position relative to the etheric bond, compared with the *ortho* position in compound 12, which significantly affects the potency of the binding. Compounds 13, 23, and 24 were low-affinity inhibitors of monocyte transmigration. Compound 13 has two significant structural differences, compared with compound 12. First, two methyl groups are located at *ortho* positions relative to the etheric aromatic group. Second, the benzyl ester moiety and the trioxotetrahydropyrimidin fragment are

located at *para* positions relative to each other. Compounds 24 and 23 do not have any methylated substitutions on the benzyl ring and the aromatic orientation of the benzyl ester relative to the etheric bond is at the *meta* position, compared with *para* in compound 12. Thus, these differences might be responsible for reducing the inhibitory activity of both compounds. Compounds 1–3, 14, and 22 were inactive. Compounds 2 and 3 contain two rings: one is trioxotetrahydropyrimidin and the other is a benzylidene motif; both are similar to compound 12. However, compound 12 has an additional third aromatic substituted ring and both compounds 2 and 3 lack this structural moiety. These data highlight the importance of the third aromatic ring for biological activity. Compound 1 is the most rigid molecule synthesized with intra-cyclization, affording saturated four-member ring molecules that reduce activation. Finally, compounds 14 and 22, which lack both *t*-butyl substitution, and methylester, which are critical for the activity, exhibited no biological activity.

Based on these results, it could be concluded that the activity of the identified compounds was via inhibition of the transendothelial migration process and that the effect was not attributed to the adhesion level of monocytes relative to the endothelial cells. The dose response effect of compound 12 was investigated in the monocyte/HUVEC system by an identical flow assay (Movie 2). We chose this molecule as a lead compound for further biological investigation and an in-depth study. Serial dilutions of compound 12, starting from 100  $\mu$ M to 3 nM, were used to establish the concentration that would give a 50 percent inhibition ( $IC_{50}$ ) using the monocyte transmigration flow assay (Fig. 4). As we have already observed in the first screening, complete blocking of monocyte transmigration was achieved at a concentration range of 30 to 100  $\mu$ M, whereas partial blocking was achieved at concentrations as

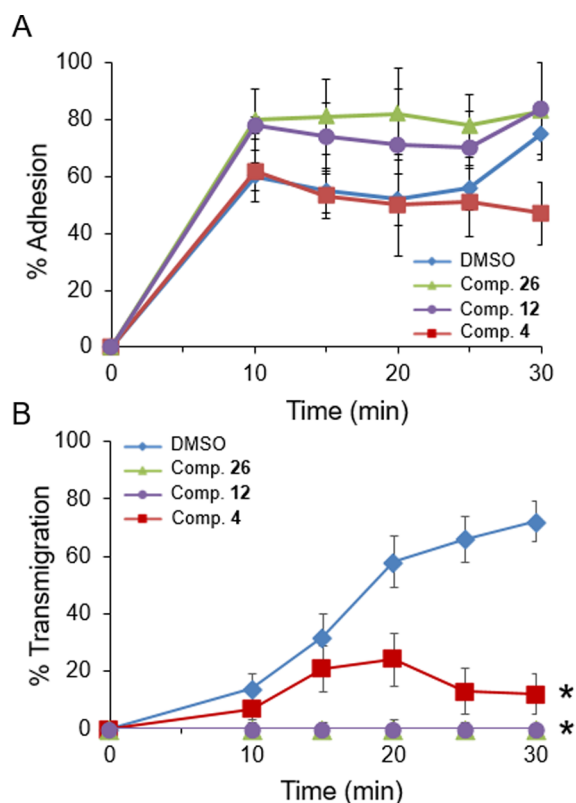


**Fig. 3.** Adhesion (sub-Figure A) and transmigration (sub-Figure B) patterns of human monocytes co-cultured on TNF- $\alpha$ -activated HUVECs under flow in the presence of compounds 12 (purple line), 26 (green line), and 4 (red line). Co-culture was treated as described in Fig. 2 (the time was shorter: 30 min, DMSO is denoted by the blue line),  $n = 3$ . Mean  $\pm$  SE,  $*P \leq 0.05$ .

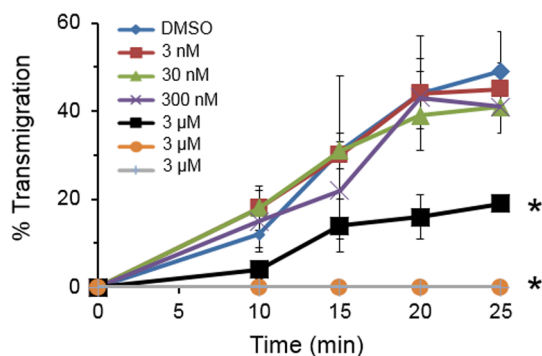


**Fig. 4.** Dose response effect of compound 12 on monocyte transmigration on the surface of HUVECs. Co-culture was treated as described in Fig. 3 by increased concentrations of compound 12; 3 nM (red line), 30 nM (green line), 300 nM (purple line), 3  $\mu$ M (black line), 30  $\mu$ M (orange line) and 100  $\mu$ M (gray line). DMSO (blue line),  $n = 3$ . Mean  $\pm$  SE,  $*P \leq 0.05$ .

low as 3  $\mu$ M. The compound lost its activity at concentrations below 300 nM. The  $IC_{50}$  value for compound 12 was 2.4  $\mu$ M, with no indication of cell toxicity at higher concentrations.

To determine whether our compound affected lymphocyte trafficking, compound 12 was tested in a T lymphocyte recruitment assay. Compound 12 had a profound effect on both adhesion and transendothelial migration. Similarly to monocytes, T cell transmigration was completely blocked by compound 12 at a concentration of 30  $\mu$ M (Fig. 5). Compound 12 was also tested in a novel B lymphocyte recruitment assay. For this purpose, a well-known drug Tysabri © (Natalizumab), an anti- $\alpha 4 \beta 1$  integrin antibody, which blocks T cell recruitment, was used as a control [45–48], as shown in Fig. 6 and Movie

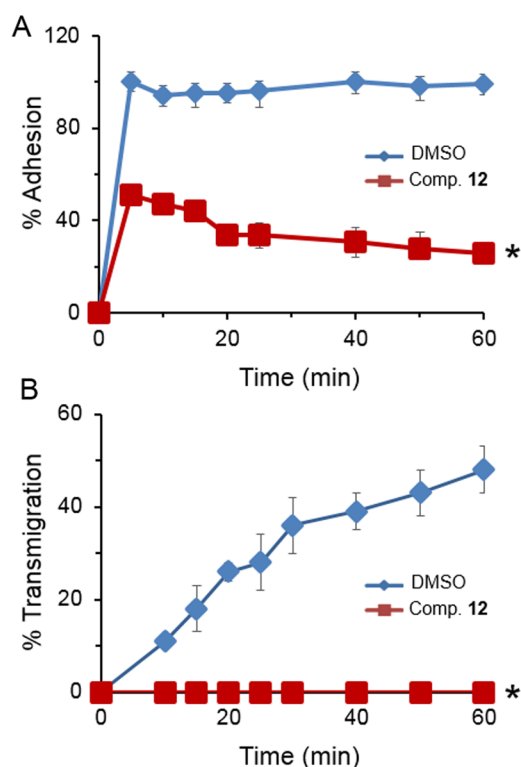


**Fig. 5.** Effect of compound 12 on T cell recruitment. Co-culture was treated as described in Fig. 4 (only for a longer time: 60 min) by compound 12 (at 30  $\mu$ M concentration red line) and by DMSO (blue line). Panel A represents the captured T cells. Panel B represents the % of T cell transmigration,  $n = 3$ . Mean  $\pm$  SE,  $*P \leq 0.05$ .

3. In our hands, compound 12 also had a potent effect on B cell recruitment, blocking both B cell adhesion to vascular endothelium and transendothelial migration. Compound 12 contrasted with Tysabri in an unexpected manner. Whereas Tysabri has been described as blocking T cell trafficking, it had no effect on the number of B cells recruited. It had only a moderate effect on the blockade of B cell adhesion to endothelium vascular; however, this was in contrast to the efficiency of adherent B cells transmigrating at a higher rate. The net effect was that the number of transmigrating B cells in the ablumen of HUVECs was identical to that of the control. This could occur for a number of reasons (e.g., adhesion blockade of a specific B cell subset); the profile of the adherent versus the transmigrated B cells is being actively investigated. This observation has many implications regarding how this translational approach can impact early drug development; for example, we found that despite the poor blockade effect on B cells' effect on Tysabri, it is still a very effective drug for treating MS and other inflammatory conditions.

Based on these observations, we propose that compound 12 interacts with vascular or leukocyte adhesion receptors that support leukocyte trafficking. Therefore, we thought that compound 12 would compete with an antibody for binding with three well-known adhesion proteins: MAdCAM-1, vascular cell adhesion protein 1 (VCAM-1), and junction adhesion molecule 1 (JAM-C). Commercially available ELISA kits were used for this determination using HeLa (cervical carcinoma) and Jeko-1 (mantle cell lymphoma) cell lines. Indeed, both types of cells are not ideal *in vitro* models for inflammatory/auto-immune diseases. However, HeLa cells express a constitutive level of MAdCAM-1 and VCAM-1 on their plasma membrane [49,50]. We planned to detect the possible inhibition by compound 12 of the binding between MAdCAM or VCAM-1 and their specific ligands (provided by the kits). The use of HeLa cells was recommended by the provider of the kits. In an identical assay we used Jeko-1 cells to test eventual blocking of JAM-

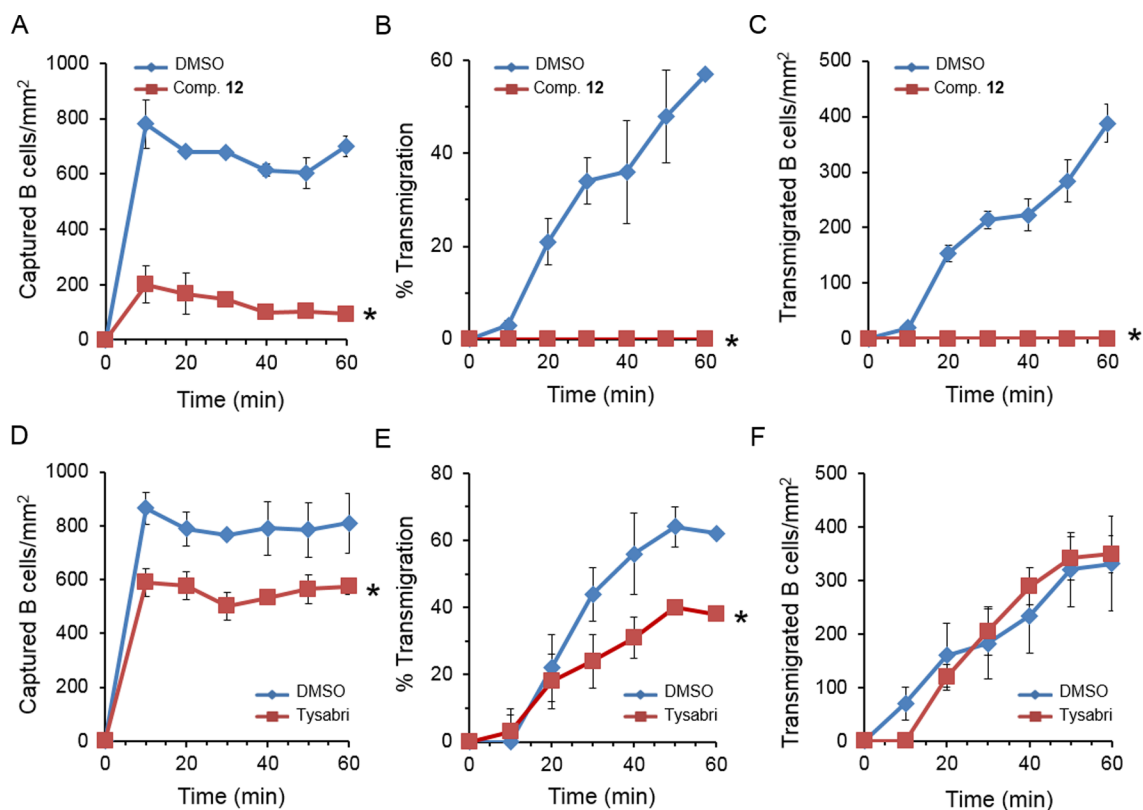


**Fig. 6.** Effect of compound 12 and Tysabri on B cell recruitment. Co-culture was treated as described in Fig. 2 (only for a longer time: 60 min) by compound 12 or by Tysabri (red line), both at a 30  $\mu$ M concentration, in both experiments DMSO was added to control samples, (blue line). (Panels A, B, C) indicate the effect of compound 12 and (Panels D, E, F) indicate the effect of Tysabri. Panels A and D represent the captured B cells. Panels B and E represent the % of B cell transmigration and Panels C and F represent the transmigrated B cells,  $n = 3$ . Mean  $\pm$  SE, \* $P \leq 0.05$ .

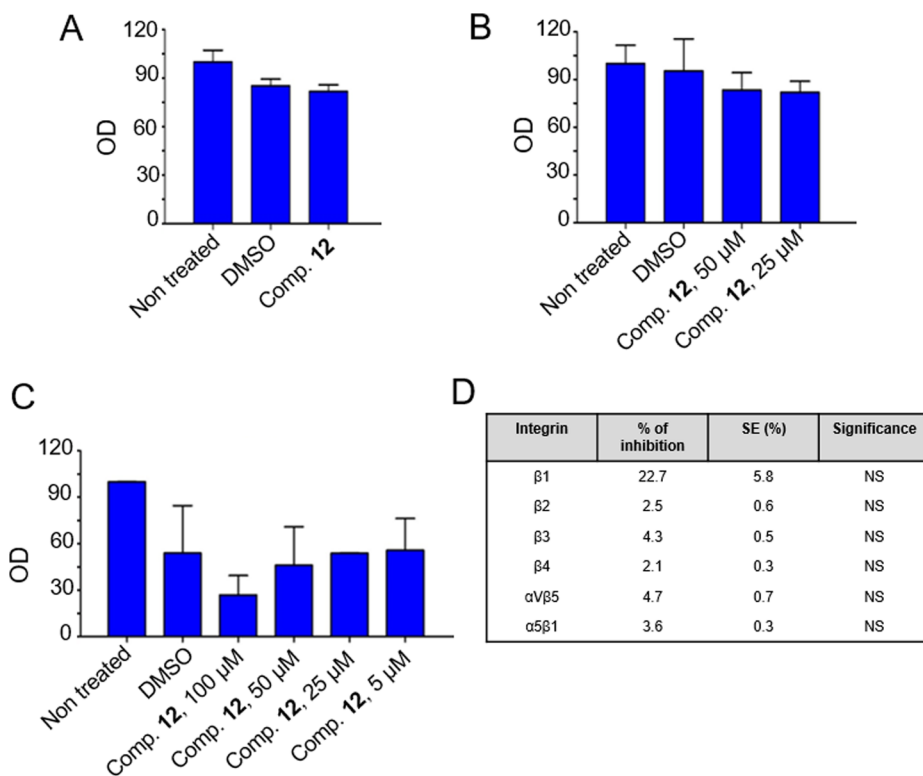


**Fig. 7.** Investigation of the possible inhibitory effect of compound 12 on the binding activity of different adhesion proteins using commercially available kits. (A) JAM-C, compound 12 was used at 30  $\mu$ M. (B) VCAM-1, (C) MAdCAM-1. (D) Panel of integrins,  $n = 6$ , Mean  $\pm$  SE, no significant differences were observed (NS, none significant).

C binding by compound **12** [51]. Fig. 7A, B and C shows that compound **12**, at a concentration at which it displayed total inhibition of monocyte transmigration, did not reduce the binding activity of these three tested proteins to their specific antibodies. In addition, Jeko-1 cells were used for identification of possible effect of compound **12** on the binding between set of integrins to their antibodies. A commercial available kit for measurement of the integrins binding was used (Fig. 7D). Also in this assay no competition between compound **12** and antibodies were detected. Obviously, we cannot draw any conclusions based on the negative results obtained in those experiments. To detect a decreased binding between a protein and its antibody in the presence of compound **12** might be possible only if they compete for the same epitope (the binding site of compound **12** is unknown), thus the lack of effect can be still explained by different epitopes of binding for the antibody and compound **12**.

The next question was: “Does compound **12** target white blood cells or endothelium, or both?” We therefore developed a strategy where monocytes and HUVEC cells were treated separately with a test compound, before co-culture in the flow assay chamber. Treatment of monocytes only, blocked monocyte transmigration (100%). Pre-treatment of endothelium by compound **12** only before flowing the monocytes, induces rapid reverse transmigration when monocytes were subsequently flown of the endothelium (Supporting Information Fig. S2A). This effect might explain the potent therapeutic effect of compound **12**, which we identified *in vivo* (discussed below) and the ability of compound **12** to revert existing inflammation. Targeted reverse leukocyte transendothelial migration would be a novel mechanism in treatment of autoimmune diseases that would raise a lot of interest. Leukocyte retention in tissue is a key factor in chronic disease and drives in human chronic inflammation. Bringing leukocytes back into the blood stream by reverse transendothelial migration could resolve the inflammation. Additional *in vitro*-related results indicated phenotypic manifestations of a distinctive movement within the HUVEC intercellular junctions observed after treatment with compound **12**. We termed this manifestation as “Fluttering”, because it was characterized by a rapid fluctuating movement (similar to butterfly wings) at the intercellular junctions of adjacent HUVECs, and predominantly within the tricellular corners. This was associated with absence of leukocyte adhesion or migration within these regions (Supporting Information Fig. S2B and Movie 4). “Fluttering” was observed in all HUVECs co-cultured with monocytes that were treated with compound **12**. In all cases, junctional integrity was maintained, and no physical breakdown was observed at the endothelial intercellular contacts. This therefore represents a phenotype that is consistent with a profound disruption in leukocyte transmigration.

### 2.3. *In vivo* studies of leukocyte migration and inflammatory pathologies

Having identified an anti-inflammatory effect *in vivo*, we tested compound **12** in a series of toxicity studies. To increase the administered dose and to avoid using dimethyl sulfoxide (DMSO) as a solvent, a simple methylcellulose-based formulation was developed as part of this study. Methylcellulose is an FDA-approved component for medical formulations and in the concentrations used for this study (0.332%), methylcellulose has been shown to be inert [52]. Eight experimental groups with five female 6–7-week-old C57BL/6J mice were treated with compound **12** and one control group with non-treated (naïve) mice was used. Mice were administered a daily application of compound **12** suspension at 5, 10, and 15 mg/kg by intraperitoneal injection (IP) or at 10, 20, and 30 mg/kg by oral gavage (PO) for 7 days. Mice from all experimental groups were observed for signs of toxicity immediately post dosing and following 2 h post-administration daily. After 24 h of the last administered dose, the mice were euthanized. Whole blood was collected and analyzed for biochemical markers, white/red blood counts, and white blood cell differentiation. Liver, spleen, lungs, heart, and kidneys were collected from each mouse and fixed with 4%

buffered formalin for future mounting in paraffin blocks. Sections from each organ of each animal were then stained with Hematoxylin/Eosin (H/E) and histological evaluation of the tissue was performed by microscopy to identify signs of toxicity. No significant changes in white and red blood were observed in blood from mice treated with compound **12** in both administered routes, as shown in Supporting Information Figs. S3 and S4. In addition, all biochemical tests on blood from mice treated with compound **12** confirmed that there were no signs of toxicity, as shown in Supporting Information Figs. S5, S6, and S7. Macro-evaluation of mouse tissues also revealed no significant changes in tissue morphology in animals treated by compound **12**, as shown in Supporting Information Figs. S8 and S9.

In addition, a good laboratory practice (GLP) toxicity experiment was also conducted. Compound **12** was administered orally, daily for 28 days to C57 black mice, in three doses. The maximal dose was supra pharmacological (200 mg/kg/day). The detailed protocol is presented in the Supporting Information. The main conclusion, which was derived from the study, is that compound **12** has no toxic effects. Body weight, clinical observations, necroscopy results, and blood tests were similar in treated and non-treated compound **12** mice.

The possible therapeutic effect of compound **12** was evaluated in an acute inflammation model of IBD/Crohn’s disease. C57BL mice were treated with dextran sulfate sodium salt (DSS) to induce colitis [53]. On day 5, water containing DSS was changed to regular drinking water and treatment with compound **12** was initiated. Compound **12** was administered at 15 mg/kg by intravenous injection (IV), IP, or subcutaneous injection (SC) injections using a q3w regimen (administered 3 times per week) and at 30 mg/kg by PO using a qd regimen (once daily). The treatment was continued for 10 days and thereafter, mice were euthanized. For determining the severity of the disease and the possible therapeutic effects of compound **12**, a disease activity index (DAI), based on the methods reported by Park et al. [54], was applied. The DAI score was calculated as the sum of the weight loss score, the diarrheal score, and the hematochezia score (Table 1).

After 10 days of treatment, and an additional 24 h after the last dose was administered, a disease activity index in all experimental groups was estimated. The obtained results were summarized in Fig. 8. Compound **12** significantly decreased the index in all four treated groups. The maximal effect was observed in the PO-administered mice; however, this may be because of the higher dose (30 mg/kg versus 15 mg/kg), which the PO-administered mice received compared to other mice that received compound **12** by IV, IP, or SC. It is important to mention that the additional autopsy examination of mouse colon samples revealed that the colon length was shorter by approximately 2 cm in all treated groups compared with the untreated animals. In addition, the presence of gross blood in the stool or anus and the formation of a stool that readily becomes paste on the anus were not detected in the treated groups compared with the control mice. In general, colons treated by compound **12** mice looked almost identical to those of naïve mice (Fig. 9A and B). A histological score was based on the parameters reported by Park et al. [54] and the score was significantly lower in mice treated with compound **12**, as shown in Fig. 9C.

Having established the striking therapeutic effect of compound **12**

**Table 1**  
Scoring criteria for the disease (IBD) activity index.

Score	Weight loss (%)	Stool consistency <sup>b</sup>	Hematochezia <sup>a</sup>
0	None	Normal	Absence
1	0–10		
2	11–15	Loose stool <sup>b</sup>	
3	16–20		
4	≥20	Diarrhea	Presence

<sup>a</sup> The presence of gross blood in the stool or anus.

<sup>b</sup> The formation of a stool that readily becomes a paste on the anus of a mouse.

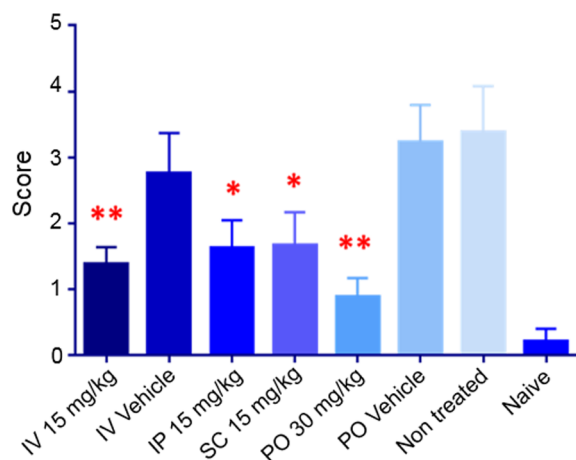


**Fig. 8.** Effect of compound **12** on the DAI score in IBD/the Crohn's disease mouse model. The experiment was conducted as described in the Results section. After 10 days of treatment, and an additional 24 h after the last administered dose, a disease activity index in all experimental groups was estimated.  $n = 3$ . Mean  $\pm$  SE, \* $P \leq 0.05$  compared to treatment by vehicle control, \*\* compared to non-treated control. ANOVA test.

in an acute IBD model, we also tested the effect of compound **12** in a chronic inflammatory multiple sclerosis model in mice. Female 7–8-week-old C57BL/6J mice were immunized with an emulsion of myelin oligodendrocyte glycoprotein (MOG) in complete Freund's adjuvant (CFA) according to standard protocols, followed by administering pertussis toxin (PTX) in phosphate buffer solution (PBS) [55]. After the onset of experimental autoimmune encephalomyelitis (EAE) after 9 days, mice were assigned by enrollment to groups, one at a time, as

**Table 2**  
EAE clinical score.

Score	Clinical manifestation
1	Limp tail
2	Partial hind leg paralysis
3	Complete hind leg paralysis
4	Complete hind and partial front leg paralysis
5	Moribund

soon as they showed the first signs of EAE (paralysis score 0.5–1). The treatment group was administered compound **12** at 15 mg/kg dose using a q3w regimen by SC injections. The mock-treated (vehicle) control group was administered a volume of solvent similar to the treated group. The body weight of animals was determined prior to the experiment and the administered volume of compound **12** formulation was adjusted according to the body weight. The EAE score (the severity of the disease) was calculated based on criteria shown in Table 2. Besides the clinical score (which mirrors the neurological symptoms), the body weight of each mouse was measured as an additional parameter for estimating the possible therapeutic effect of compound **12**. Fig. 10A shows that starting already from the tenth day, the onset of the disease in mice treated with compound **12** was delayed, and that the body weight at day 20 of treatment returned to normal. This contrasted significantly with non-treated and control group mice where the loss in body weight differed by as much as 4 g approximately. These differences closely correlated with the measured changes in clinical scores. Starting from the 10th day, mice treated with compound **12** showed no increase in the disease score and by day 20, the score even decreased to score values of 2 to 1.5. In contrast, non-treated and control mice reached a score above 2.5 in the same timeframe (Fig. 10B).

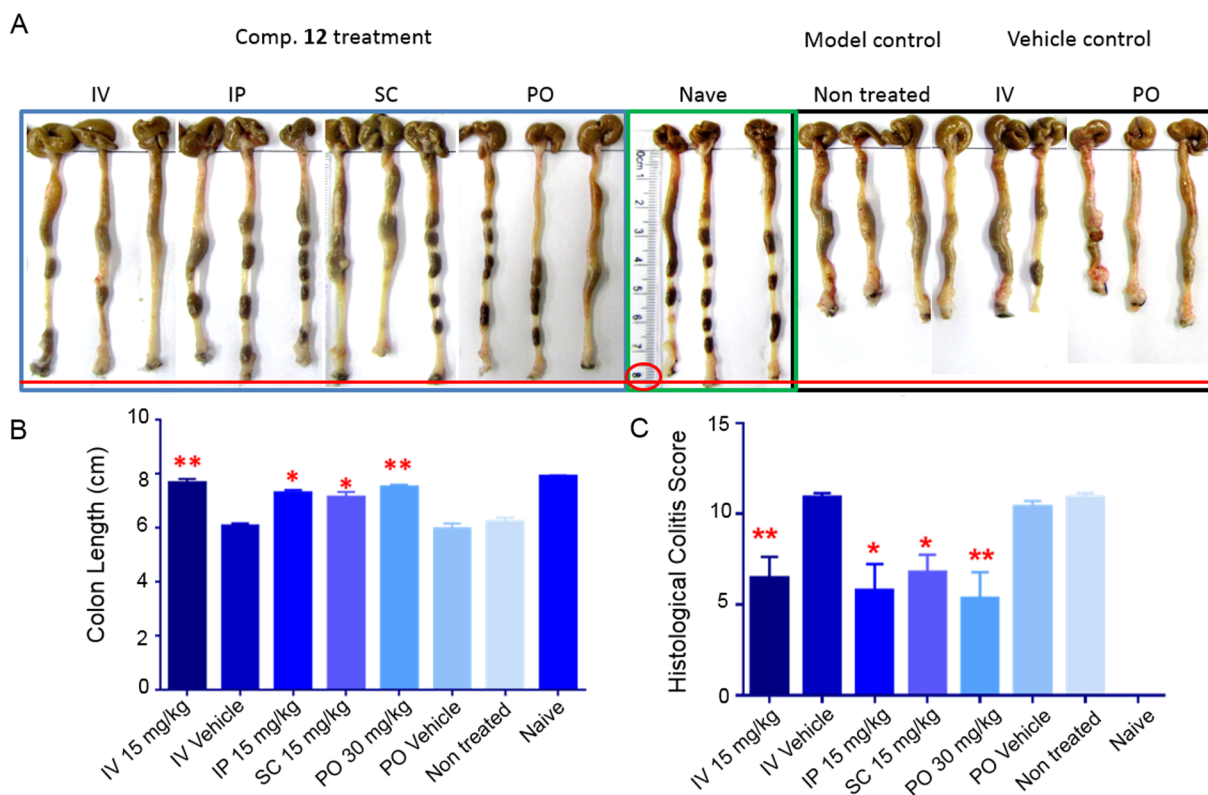


**Fig. 9.** Effect of compound **12** on the length and histology of colon in the Crohn's disease mouse model. (A) The experiment was conducted as described in the Results section. After 10 days of treatment, and an additional 24 h after the last administered dose, mice were euthanized; their colons were isolated, fixed, and photographed. (B) Colon length measurement. (C) The intestinal lumen was investigated (mucosa, gross lesions, the architecture of the epithelial structure, the content of inflammatory cells (mostly lymphocytes) within the lamina propria). Lymphoid follicles were investigated in caecum submucosae.  $n = 3$ . Mean  $\pm$  SE, \* $P \leq 0.05$  compared to those treated by vehicle control, \*\* compared to the non-treated control.

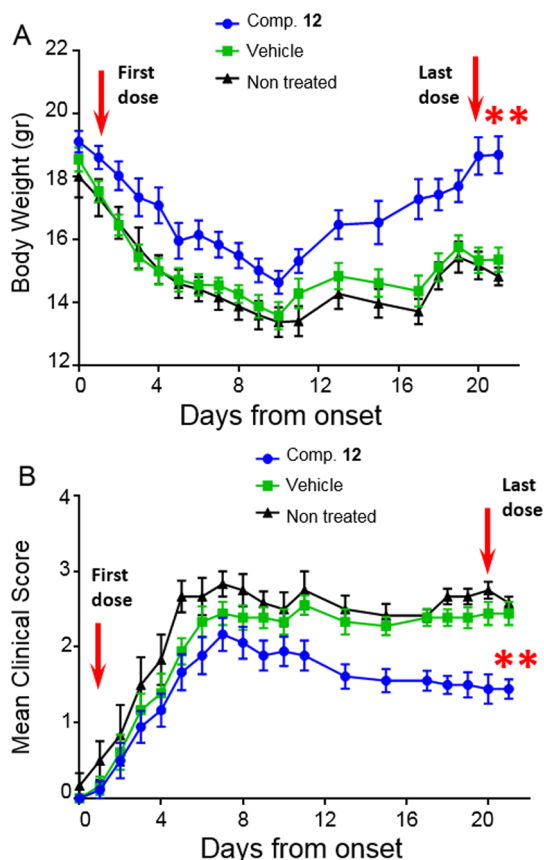


**Fig. 10.** Effect of compound 12 on the mouse body weight and paralysis score. The experiment was conducted as described in the Results section. During the 21 days of treatment, the body weight, (A), and the paralysis clinical score, (B), were measured daily in all experimental groups. Data shown represent the Mean  $\pm$  SEM,  $n = 10$ , \* $P < 0.0001$  compared to those treated by vehicle control, \*\* compared to the non-treated control.

We then decided to investigate the effect of compound 12 in chronic inflammatory pathology, which is related to insulin resistance and the metabolic syndrome: non-alcoholic fatty liver dystrophy (NAFLD), which in the last decade has attracted much attention owing to a forecast of increased frequency in the USA, Europe, and other industrialized countries. The classical *in vivo* model for NAFLD was conducted in mice placed on a high-fat diet for a prolonged time period to simulate a western diet (14 weeks prior to treatment initiation). Compound 12 was administered on day 85 of the fat diet (15 mg/kg, for SC and IP, 30 mg/kg for PO), three times per week for 65 days. Compound 12 significantly reduced the body weight of mice in all administered routes (Supporting Information Fig. S10). After euthanasia of the mice and a histopathological analysis of the livers, it was found that compound 12 dramatically reduced the level of fat in the liver almost to the normal histology (the SC administration results are shown in Fig. 11A). In addition, even the amount of fat in the physiological depot (mesenteric space) was significantly reduced because of compound 12 administration (Fig. 11B). The activity score of the disease in the mice under SC administration was also similar to that of the naïve mouse group (zero values in both categories, Fig. 11C). IP and PO-administered compound 12 likewise significantly reduced the disease score. Compound 12 also significantly decreased the liver weight after treatment by all routes of administration mentioned above, as shown in Fig. 11D. Finally, the mesenteric fat mass measurements were also significantly reduced by compound 12 treatment given PO, SC, and IV (Fig. 11E).

It is important to mention that already in 2011 Liang Ma et al. reported the significant effect of trioxotetrahydropyrimidin derivatives

(however, substantially different ones from our reported compounds are described here) in the nonalcoholic fatty liver disease mouse model [56,57]. The authors proposed that their compounds would activate peroxisome proliferator-activated receptor (PPAR- $\gamma$ ); however, they did not prove this hypothesis at the molecular level and did not test the effect of the lead compound on leukocyte transmigration [58].

Our final evaluated chronic inflammatory *in vivo* model investigated the effect of compound 12 on rheumatoid arthritis, an autoimmune disorder that can be induced in mice by injection of collagen (collagen-induced arthritis, CIA) [59]. To this end, male DBA/1 mice (7–8 weeks of age) were injected with collagen type II (CII) + CFA emulsion on day 0 by SC. On day 21 the animals received the same amount of the emulsion as a booster. On day 22, the mice were randomized, and treatment was initiated. On days 0, 22, and 43, the paws of all mice were measured using calipers to establish baseline and experimental end-point values for paw thickness. The CIA scoring was conducted on a scale of 0 to 16 (0 to 4 for each paw, adding the scores for all 4 paws). For this study, compound 12 was administered IP (15 mg/kg, four times per week) for 21 days. Fig. 12 shows that after two weeks, compound 12 significantly reduced the clinical score in the treated mice. This effect was observed for the duration of the experiment. In addition, compound 12 also improved local arthritis manifestations, in both fore and hind limbs, where the thickness of both limbs was significantly reduced (Fig. 13A and B). Finally, all limb pathologies were assessed by histology using hematoxylin and eosin (H&E) stains in paraffin-embedded sections. Joints were scored for inflammation, cartilage damage, pannus formation, and bone resorption on a scale of 0 to 3 for each readout (Supporting Information Fig. S11). In Fig. 13C the individual score values represent the summarized results. Compound 12 decreased the total histological score by more than 50%. The body weight of treated animals remained relatively constant during the administration of the compound; thus, the decreased tissue thickness was not related to weight loss and a perceived reduction of stress on the associated joints (Supporting Information Fig. S12).

#### 2.4. *In silico* study of PECAM-1 binding

Since we did not see that compound 12 inhibits antibody binding to MAdCAM, despite that the trioxotetrahydropyrimidin derivatives developed by Harriman et al. affected this protein, we hypothesized that compound 12 may have a different mechanism of action. We conducted *in silico* experiments to investigate and identify a possible molecular target of compound 12. One of the vascular adhesion molecules that appeared as such a target is the PECAM-1. The role of this receptor in inflammation, leukocyte transendothelial migration, and cancer has highlighted a number of opportunities in drug development. PECAM-1 has been shown to be involved in the late-stage progression in cancer, highlighting a potential mechanism in disease stratification, which is dependent on the stage of treatment [60]. PECAM-1 is also known to regulate T cell trafficking into the central nervous system (CNS) during critical pathologies, demonstrating that targeting this receptor may block multiple cell populations in both inflammation and cancer [61]. PECAM-1 not only resides at the junction; it is also a constituent of a recycling compartment of endothelial cells, termed the lateral border recycling compartment (LBRC), which modulates the transmigration of leukocytes through the endothelial cell-cell junction [62]. The active and inactive compounds were docked into the predicted binding sites of the monomeric and dimeric structures of PECAM-1 in order to determine which site can best distinguish between active and inactive compounds measured by the area under the receiver operating characteristic (ROC) - curve, which ranges between 0.5 for a separation not better than random, and 1 for a perfect separation, (Fig. 14A). ROC values calculated for sites on the monomeric structure were all below 0.6, thereby ruling out these sites (*data not shown*) [56]. On the other hand, one of the sites identified on dimeric PECAM-1 (site 4) produces an AUC (area under the curve)-ROC value of 0.73 (Fig. 14B) with lower

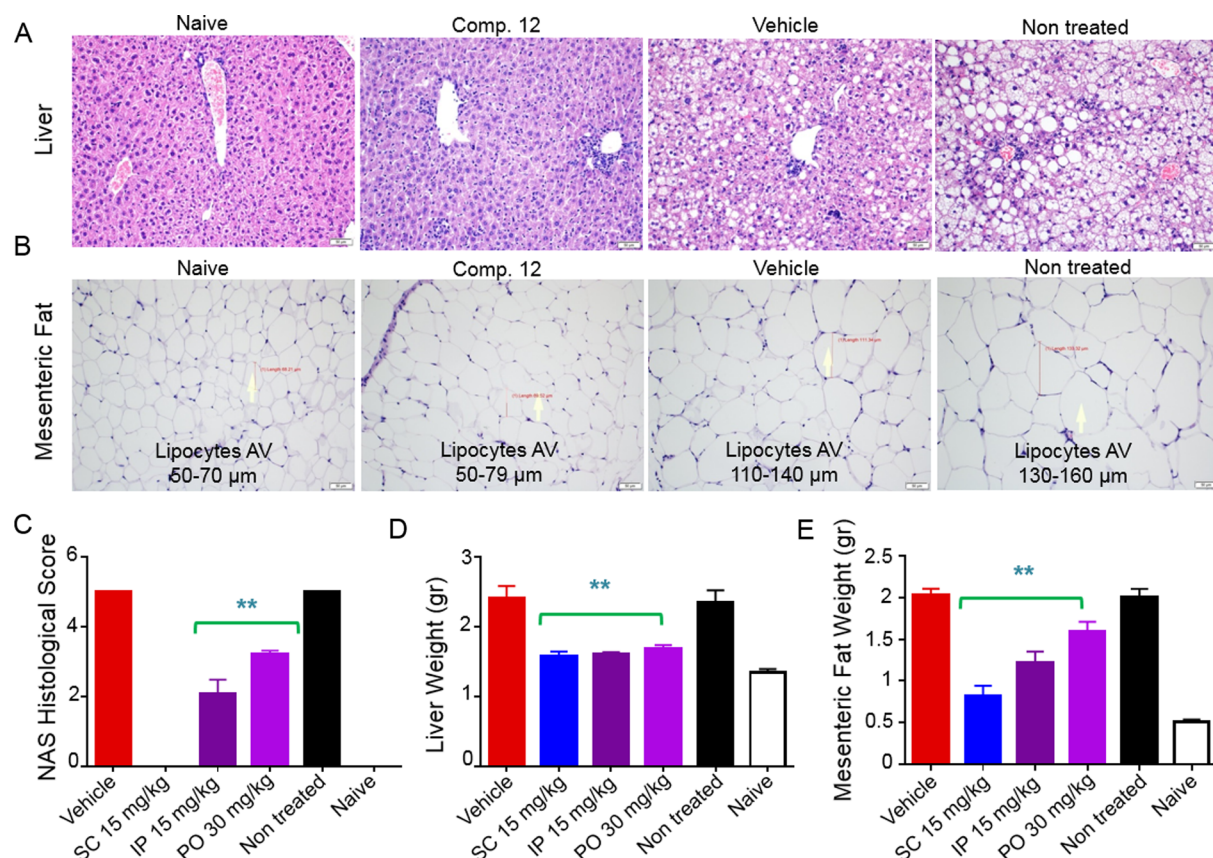


**Fig. 11.** Effect of compound 12 on fat accumulation in the NAFLD mouse model. Male mice (3–4 weeks of age) were fed ad libitum a high-fat diet, no high-carbohydrate diet (modified WD) with 42% kcal from fat containing 0.1% cholesterol (Harlan TD.88137) with normal water (without a high fructose-glucose solution) for 14 weeks prior to initiating treatment. Control mice were fed with a standard chow diet (CD, Harlan TD.7012) with normal water (NW). Compound 12 was administered by IP injections at 15 mg/kg dose using a q3w regimen for two months. Liver (A) and mesenteric fat (B) histologies were assessed using H&E stains in paraffin-embedded sections. (C) In addition to IP injection, compound 12 was also administered by SC (15 mg/kg) and PO (30 mg/kg). Steatohepatitis was defined by the presence of steatosis, inflammation, and hepatocellular ballooning, according to the FLIP algorithm. The severity of steatosis, lobular inflammation, and hepatocellular ballooning was scored using the CRN criteria. The NAS was calculated by adding the scores of steatosis (the maximum score is 3), which is defined by more than 66% of hepatocytes containing fat droplets, with lobular inflammation (the maximum score is 3), which is defined by > 4 foci/200 field hepatocyte ballooning (maximal score 2), which is defined by many cells/prominent ballooning. The maximum NAS score combining all three features is 8. In all mice, hepatocyte ballooning, as well as portal and perisinusoidal fibrosis was not detected. (D) Liver weight. After 60 days of the treatment, livers were isolated and weighed. (E) Mesenteric fat weight. After 60 days of treatment, mesenteric fat was isolated and weighed. Data shown represent the Mean  $\pm$  SEM,  $n = 8$ ,  $n = 6$ ,  $**P < 0.002$ . ANOVA test. The double asterisk shows a significant difference in the obtained results compared to the non-treated control and also to the vehicle-treated group.

values obtained for all other sites (0.64, 0.52, 0.65, and 0.37 for sites 1, 2, 3, and 5, respectively). Thus, we hypothesize that site 4, located at the interface between the two monomers of PECAM-1, can potentially serve as the binding site for compound 12 (Fig. 14C and D). If indeed compound 12 binds to PECAM-1 but only to its activated form (dimer), such a difference may represent a very important advantage to clinics, because it suggests that treatment with compound 12 might selectively block PECAM-1 in the vascular region and not on platelets. This theoretical observation might also explain the lack of general toxicity of compound 12 in mice [63]. It is important to mention that PECAM-1 knockout (KO) mice have proinflammatory phenotype results, for example, in atherogenic diet-induced steatohepatitis [60]. However, also a high level of PECAM-1 leads to increased transmigration of immune cells to organs [64,65]. In our case, compound 12 prevented the development of NAFLD in mice as we showed above. Therefore, other molecular targets of compound 12 might be involved in its biological effect. The exact mechanism of action of compound 12 is currently under investigation.

#### 2.5. $^{19}\text{F}$ NMR detection of fluorinated compound 12 (compound 30) in HeLa cell versus PC12 cell

Fluorine exhibits an excellent NMR trace ability and it is totally absent in animal cells and fluids [66,67]. Thus,  $^{19}\text{F}$  NMR is an intensive use in drug discovery as a pharmacokinetic and pharmacodynamics tool [68]. To further evaluate the possibility that compound 12 binds to PECAM1, we introduced a fluorine atom instead of hydrogen in the *ortho* position in the second aromatic ring of compound 12 (Scheme 4). We supposed that if the compound binds to PECAM1, we should detect  $^{19}\text{F}$  NMR signal only in the cells which express the protein. PECAM1 is in use as a specific marker of endothelial cells in different immunohistological techniques and it is absent in neurons. Thus, we planned to expose both types of cells to compound 30 and conduct  $^{19}\text{F}$  NMR measurements to the obtained lysates. Due to technical limitations instead of endothelial cells, we used epithelial cells (HeLa cell line) versus neuronal PC12 cells. Such exchange was possible, because of the fact that HeLa cells express PECAM1 selectively only on the plasma membrane [69,70]. Indeed, in exposed to compound 30 HeLa cells,  $^{19}\text{F}$  was detected (Supporting Information Fig. S13) and in PC12 (neuron-like

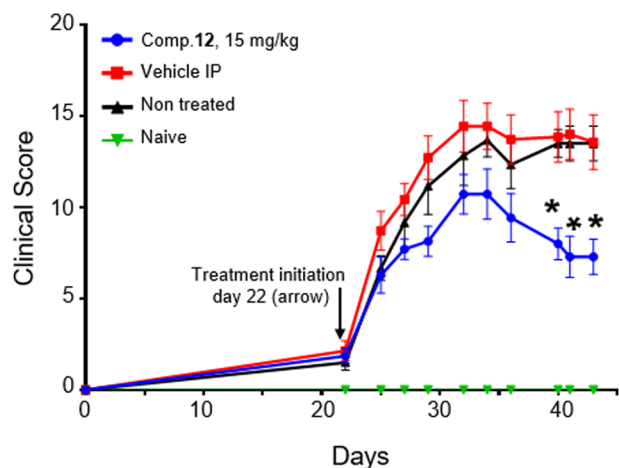


**Fig. 12.** Effect of compound **12** on the CIA score in the arthritis mouse model. Male DBA/1 mice (7–8 weeks of age) were injected with CII + CFA emulsion on day 0 (SC) at the base of the tail with a volume of 0.05 mL/animal. On day 21 the animals received the same amount of the emulsion as a booster. On day, 22 mice were randomized and the treatment was initiated (SC injections with a 15 mg/kg dose using the q3w regimen. On days 0, 22, and 43, the paws of all mice were measured using calipers to establish baseline and end point values for paw thickness. The CIA scoring was on a scale of 0 to 16 (0 to 4 for each paw, adding the scores for all 4 paws). Data shown represent the Mean  $\pm$  SEM,  $n = 8$ ,  $n = 7$  (not treated). \* $P < 0.002$ . ANOVA test.

cells),  $^{19}\text{F}$  was not detected at all. Those results might indirectly support our hypothesis that compound **12** binds to PECAM1.

## 2.6. PK study

Preliminary PK study was conducted in C57 black mice. Compound **12** was administrated PO by a single dose (gavage, 50 mg/kg) in the minimal amount of DMSO (70  $\mu\text{L}$ ). The level of the compound was measured by LC-MS after the extraction from the plasma by chloroform (due to high lipophilicity of the molecule). The compound reaches the peak concentration in the blood after 2.5 h (around 15  $\mu\text{M}$ ) and after 9 h the level of the compound was undetectable (Fig. 14S). Suggesting that compound **12** might be the main pharmacological active specie, although the broad PK study with identification of possible active metabolites are still needed.

## 3. Conclusions

Modified trioxotetrahydropyrimidin scaffolds were used for

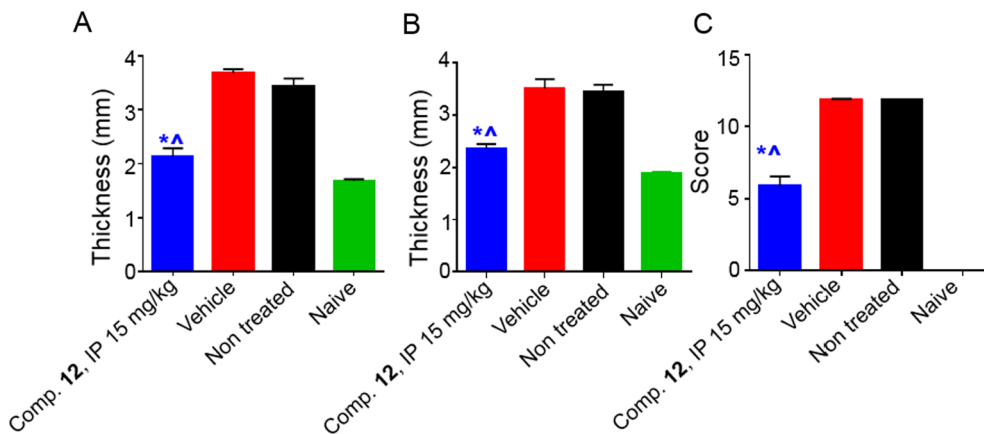


**Fig. 13.** Effect of compound **12** in the Collagen-Induced Arthritis (CIA) model in DBA/1 mice (limb thickness and histological score). (A) Fore limb thickness, (B) Hind limb thickness, (C) Histological score. Data shown represent the mean  $\pm$  SEM,  $n = 8$ . \* $P \leq 0.05$  compared to those treated by vehicle control, ^ compared to the non-treated control.

developing a leukocyte transmigration inhibitor (compound **12**). The lead compound was active in IBD/Crohn's disease, multiple sclerosis, fatty liver disease, and rheumatoid arthritis mouse models at pharmacological doses. The clinical score was improved by compound **12** by 75%, 40%, 100% and 46% respectively. Compound **12** did not exhibit any toxic effects in mice at the administered doses. Based on *in silico* calculations, we postulate that compound **12** blocks PECAM-1, its mono or heterodimeric form found in vascular endothelial junctions. Such types of molecules might therefore provide a unique possibility for developing novel classes of leukocyte transmigration blocking agents with broad therapeutic applications, especially for the treatment of acute inflammation and chronic autoimmune diseases. The exact binding partner of compound **12** now is under intensive investigation.

Beside the possible use of compound **12** as a drug candidate for the developing of novel therapeutics against auto-immune diseases or inflammation related disorders, compound **12** might also serve as a carrier for the delivery of anti-inflammatory, anti-thrombotic and antioxidant agents to the pathologically altered vasculature [71,72]. Furthermore, anchoring of some drug delivery systems to compound **12** might provide trans-endothelial delivery of drugs and genetic materials [73,74].

## 4. Experimental section

### 4.1. Materials

All chemical reagents, solvents, and acids were purchased from Acros Organic, Alfa Aesar, Bio-Lab Ltd., and Merck, and were all used as received. Anhydrous tetrahydrofuran (THF) was obtained by distillation from a boiled blue colored mix containing sodium (1% w/v) and benzophenone (0.2% w/v). Anhydrous dimethylformamide (DMF) was obtained by distillation under vacuum and stored over 4  $\text{A}^\circ$  molecular sieves. Column chromatography was performed on silica gel 60 (230–400 mesh; Merck). Analytical and preparative high-performance liquid chromatography (HPLC) (Young Lin Instruments, Anyang, Korea) were performed on LUNA C18 preparative (10  $\mu\text{m}$ , 100  $\times$  30 mm) or analytical (5  $\mu\text{m}$ , 250  $\times$  4.6 mm) columns, both from Phenomenex, Inc. (Torrance, CA, USA). HPLC purification was carried out with an increasing linear gradient of  $\text{CH}_3\text{CN}$  in  $\text{H}_2\text{O}$ . The purity of all synthesized compounds was confirmed by elemental analysis and for compounds **29** and **30** by analytical HPLC. Analytical thin-layer chromatography (TLC) was carried out on pre-coated silica gel 60 F254 (Merck) sheets using UV absorption and iodine physical adsorption for visualization. Mass spectra were recorded on a Finnigan Model 400 instrument using a QToF microspectrometer (Micromass, Milford, MA, USA), using electrospray ionization (ESI) in the positive ion mode. 6200 Series Accurate-Mass Time-of-Flight (TOF) LC/MS from Agilent Technologies (Santa Clara, CA, USA) was used for PK analysis. Data were processed

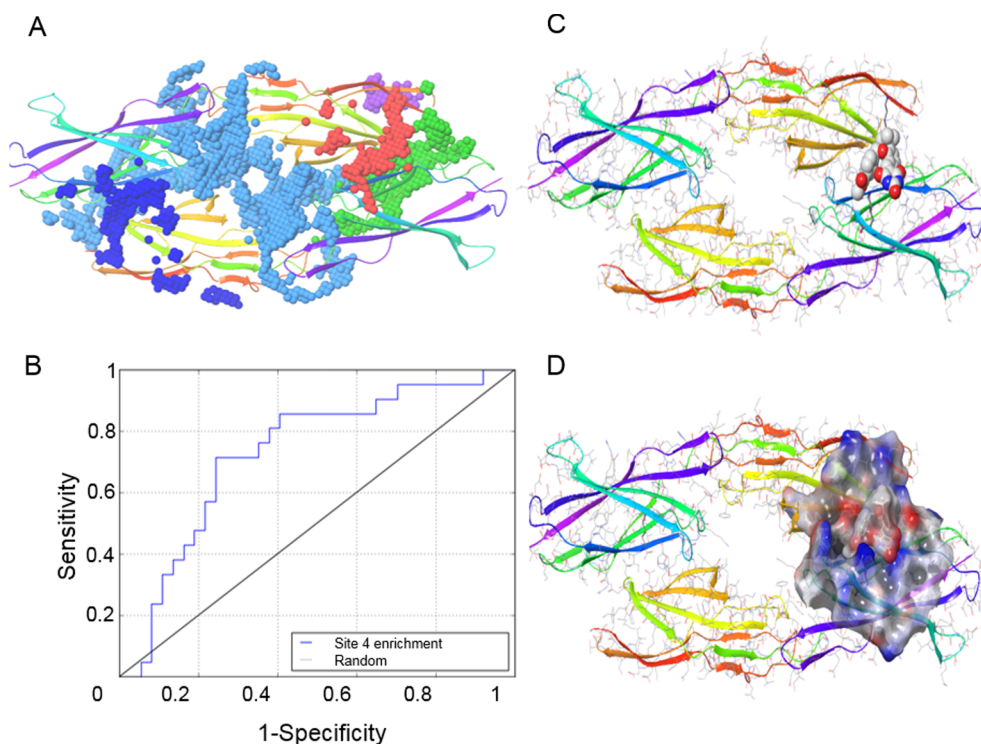


**Fig. 14.** Binding sites and the binding mode of compound **12** within the PECAM-1 dimer structure. (A) Predicted binding sites within the PECAM-1 dimer structure. Site 1: light blue, site 2: green, site 3: blue, site 4: red, and site 5: purple. The best ROC curve (calculated for 7 active and 13 inactive compounds) was obtained for site 4. (B) ROC curve (AUC of 0.73) obtained for site 4. The black 45° line represents random ranking. (C) Representation of compound **12** at binding site 4. (D) CPK representation of compound **12** at binding site 4.

using mass L-ynX ver. 4.1 calculation and de-convolution software (Waters Corp., Milford, MA, USA). High-resolution mass spectra (HRMS) were obtained using an LTQ Orbitrap XL (Thermo Scientific, Waltham, MA, USA). Melting points were measured with a Fisher-Johns melting point apparatus (Waltham, MA, USA). The  $^1\text{H}$  NMR and  $^{13}\text{C}$  NMR were recorded at room temperature on a Bruker Advance NMR spectrometer (Vernon Hills, IL) operating at 300, 400, 600, and 700 MHz and were in accordance with the assigned structures. Chemical shift values were reported relative to tetramethylsilane (TMS), which was used as an internal standard. Chemical shifts were expressed in  $\delta$  (ppm) and coupling constants ( $J$ ) in hertz. The splitting pattern abbreviations are as follows: s, singlet; d, doublet; t, triplet; q, quartet; quintet; m, unresolved multiplet due to the field strength of the instrument; dd, doublet of doublet. Dulbecco's modified Eagle's medium (DMEM), Roswell park memorial institute (RPMI) 1640 medium, fetal calf serum (FCS), L-glutamine, penicillin/streptomycin and trypsin were purchased from Biological Industries (Beth-Haemek, Israel). Heparin, hydrocortisone, DMSO, PBS tablets, Medium 199, radioimmunoprecipitation (RIPA) buffer, methylcellulose and Type II collagen were purchased from Merck-Sigma-Aldrich Chemicals (Rehovot, Israel). TNF- $\alpha$ , IFN $\gamma$ , and CXCL-12 and -13 were purchased from Peprotech, Rehovot, Israel. Endothelial cell growth supplement was from Upstate Biotechnology (Boston, MA). T-, B-, monocyte selection kits were from Miltenyi Biotec (Bergisch Gladbach, Germany). Kits for determining the blocking activity of compound **12** of JAM-C were purchased from Ray-Biotech (Norcross, GA, USA) of VCAM-1 from Abcam (Cambridge, UK), Beta Integrin-Mediated Cell Adhesion Array Kit was purchased from Chemicon (Temecula, CA, USA) and MAdCAM-1 from ELAab (Guangguguoji, Wuhan, China). The bicinchoninic acid-based protein concentration determination kit was purchased from Pierce (Waltham, MA). Santa Cruz Biotechnology supplied complete Freund's adjuvant.

## 4.2. Synthetic procedures

### 4.2.1. General procedure for the synthesis of methylated benzoates (**5**, **15** and **28**) [41]

To a solution of 4-bromomethylbenzoic acid, 3-chloromethylbenzoic acid or 4-(bromomethyl)-2-fluorobenzoic acid (2.30 mmol) in MeOH (5.6 mL), concentrated sulfuric acid (0.14 mL) was added. The resulting mixture was refluxed for 5 h. Then, the mixture was cooled to room temperature and evaporated in vacuo. H<sub>2</sub>O (20 mL) was added to the reaction mix in an ice-water bath, and the resulting solid was filtered and washed with cold water. The solid material was partitioned between Et<sub>2</sub>O/AcOEt 1:1 and Na<sub>2</sub>CO<sub>3</sub>. The organic layer was dried over Na<sub>2</sub>SO<sub>4</sub> and evaporated in vacuo to afford the products.

### 4.2.2. Methyl 4-(bromomethyl)benzoate (**5**)

The title compound was obtained starting from 3-chloromethylbenzoic acid (white powder, yield 48%):  $^1\text{H}$  NMR (400 MHz, CDCl<sub>3</sub>):  $\delta$  7.96 (d,  $J$  = 8.41 Hz, 2H), 7.40 (d,  $J$  = 8.41 Hz, 2H), 4.45 (s, 2H), 3.87 (s, 3H) ppm.  $^{13}\text{C}$  NMR (100.6 MHz, CDCl<sub>3</sub>):  $\delta$  166.28, 142.59, 129.95, 128.98, 52.10, 32.27 ppm. MS (ESI, SQ),  $m/z$  (%): (229  $^{79}\text{Br}$ , 231  $^{81}\text{Br}$ ) [M + H]<sup>+</sup>.

### 4.2.3. Methyl 3-(chloromethyl)benzoate (**15**)

The title compound was obtained starting from 3-chloromethylbenzoic acid (colorless syrup, yield 75%):  $^1\text{H}$  NMR (400 MHz, CDCl<sub>3</sub>):  $\delta$  8.06 (s, 1H), 7.99 (d,  $J$  = 7.76 Hz, 1H), 7.58 (d,  $J$  = 7.76 Hz, 1H) 7.429 (t,  $J$  = 7.76 Hz, 1H), 4.61(s, 2H), 3.92 (s, 3H) ppm.  $^{13}\text{C}$  NMR (100.6 MHz, CDCl<sub>3</sub>):  $\delta$  166.54, 137.91, 132.99, 130.73, 129.67, 129.55, 128.28, 52.23, 45.52 ppm. GC-MS (EI), 70 ev,  $m/z$  (%): 184 [M]<sup>+</sup>.

### 4.2.4. General procedure for the synthesis of **6**, **7**, **8**, **9**, **16**, **17**, **18**, and **25** [42]

A suspension of **5**, **15** or **28** (6.55 mmol) and the corresponding benzaldehydes (6.55 mmol) including potassium carbonate

(13.10 mmol), and potassium iodide (7.86 mmol) was heated at 70 °C for 5 h. The solvent was evaporated, the residue was dissolved in ethyl acetate (50 mL), washed with saturated aqueous NaHCO<sub>3</sub> solution (2 × 20 mL), water (2 × 20 mL), and brine (2 × 10 mL), dried over Na<sub>2</sub>SO<sub>4</sub>, and concentrated under reduced pressure. The crude product was purified by flash column chromatography using ethyl acetate/petroleum ether as an eluent.

#### 4.2.5. Methyl 4-((2-formylphenoxy)methyl)benzoate (6)

(white powder, yield 60%) <sup>1</sup>H NMR (300 MHz, CDCl<sub>3</sub>): δ 10.57 (s, 1H), 8.07 (d, *J* = 8.43 Hz, 2H), 7.86 (d, *J* = 7.50 Hz, 1H), 7.53 (d, *J* = 8.43 Hz, 2H), 7.76 (t, *J* = 7.50 Hz, 1H), 7.06 (t, *J* = 7.50 Hz, 1H), 7.01 (d, *J* = 8.44 Hz, 1H), 5.25 (s, 2H), 3.92 (s, 3H) ppm. <sup>13</sup>C NMR (75.49 MHz, CDCl<sub>3</sub>): δ 189.48, 166.68, 160.64, 141.18, 135.94, 130.03, 128.73, 126.85, 125.19, 121.31, 112.90, 69.76, 52.20 ppm. MS (ESI, SQ), *m/z* (%): 293.1 [M+Na]<sup>+</sup>.

#### 4.2.6. Methyl 4-((3-formylphenoxy)methyl)benzoate (7)

(yellow powder, yield 54%) <sup>1</sup>H NMR (300 MHz, CDCl<sub>3</sub>): δ 9.96 (s, 1H), 8.06 (d, *J* = 8.27 Hz, 2H), 7.54–7.44 (m, 5H), 7.29–7.22 (m, 1H), 5.17 (s, 2H), 3.91 (s, 3H) ppm. <sup>13</sup>C NMR (75.49 MHz, CDCl<sub>3</sub>): δ 191.95, 166.74, 159.01, 141.48, 137.87, 130.23, 129.96, 129.89, 127.02, 124.00, 122.11, 113.15, 69.49, 52.16 ppm. MS (ESI, SQ), *m/z* (%): 271.1 [M+H]<sup>+</sup>, 293.2 [M+Na]<sup>+</sup>.

#### 4.2.7. Methyl 4-((2-tert-butyl-6-formylphenoxy)methyl)benzoate (8)

(off white powder, yield 43%, m.p. 84 °C) <sup>1</sup>H NMR (300 MHz, CDCl<sub>3</sub>): δ 10.30 (s, 1H), 8.11 (d, *J* = 8.04 Hz, 2H), 7.75 (dd, *J* = 7.80 Hz, *J* = 1.65 Hz, 1H), 7.64 (dd, *J* = 7.81 Hz, *J* = 1.62 Hz, 1H), 7.58 (d, *J* = 8.04 Hz, 2H), 7.21 (t, *J* = 7.81 Hz, 1H), 5.12 (s, 2H), 3.94 (s, 3H), 1.44 (s, 9H) ppm. <sup>13</sup>C NMR (75.49 MHz, CDCl<sub>3</sub>): δ 190.16, 166.78, 161.26, 143.93, 141.53, 133.72, 129.99, 129.91, 128.36, 126.53, 124.37, 79.35, 52.18, 35.26, 30.86 ppm. MS (ESI) found *m/z* 349.14102 (calcd for C<sub>20</sub>H<sub>22</sub>O<sub>4</sub>: 349.14103 [M+Na]<sup>+</sup>). Anal. Calcd for C<sub>20</sub>H<sub>22</sub>O<sub>4</sub>: C, 73.60; H, 6.79. Found: C, 74.32; H, 7.03.

#### 4.2.8. Methyl 4-((4-formyl-2,6-dimethylphenoxy)methyl)benzoate (9)

(yellow powder, yield 94%, m.p. 82 °C) <sup>1</sup>H NMR (400 MHz, CDCl<sub>3</sub>): δ 9.87 (s, 1H), 8.07 (d, *J* = 8.4 Hz, 2H), 7.57 (s, 2H), 7.54 (d, *J* = 8.4 Hz, 2H), 4.92 (s, 2H), 3.92 (s, 3H), 2.33 (s, 6H) ppm. <sup>13</sup>C NMR (75.49 MHz, CDCl<sub>3</sub>): δ 191.52, 166.69, 160.86, 141.99, 132.52, 132.07, 130.75, 129.66, 127.24, 73.25, 52.13, 16.46 ppm. MS (ESI) found *m/z* 299.12793 (calcd for C<sub>18</sub>H<sub>18</sub>O<sub>4</sub>: 299.12779 [M+H]<sup>+</sup>). Anal. Calcd for C<sub>18</sub>H<sub>18</sub>O<sub>4</sub>: C, 72.47; H, 6.08. Found: C, 71.92; H, 5.87.

#### 4.2.9. Methyl 3-((2-formyl-6-methylphenoxy)methyl)benzoate (16)

(off white powder, yield 61%, m.p. 45 °C) <sup>1</sup>H NMR (300 MHz, CDCl<sub>3</sub>): δ 10.29 (s, 1H), 8.11 (s, 1H), 8.05 (d, *J* = 7.75 Hz, 1H), 7.70 (d, *J* = 7.66 Hz, 1H), 7.65 (d, *J* = 7.66 Hz, 1H), 7.49 (t, *J* = 7.66 Hz, 1H), 7.48 (d, *J* = 7.66 Hz, 1H), 7.18 (t, *J* = 7.66 Hz, 1H), 5.01 (s, 2H) ppm. <sup>13</sup>C NMR (75.49 MHz, CDCl<sub>3</sub>): δ 190.12, 166.73, 159.87, 137.71, 136.67, 132.43, 130.65, 129.70, 129.49, 128.86, 126.92, 124.72, 52.25, 15.95 ppm. MS (ESI) found *m/z* 307.09402 (calcd for C<sub>17</sub>H<sub>16</sub>O<sub>4</sub>: 307.09408 [M+Na]<sup>+</sup>). Anal. Calcd for C<sub>17</sub>H<sub>16</sub>O<sub>4</sub>: C, 71.82; H, 5.67. Found: C, 71.78; H, 5.88.

#### 4.2.10. Methyl 3-((2-formylphenoxy)methyl)benzoate (17)

(white powder, yield 44%) <sup>1</sup>H NMR (300 MHz, CDCl<sub>3</sub>): δ 10.52 (s, 1H), 8.10 (s, 1H), 7.98 (d, *J* = 7.63 Hz, 1H), 7.81 (d, *J* = 7.63 Hz, 1H), 7.63 (d, *J* = 7.63 Hz, 1H), 7.55–7.38 (m, 2H), 7.08–6.95 (m, 2H), 5.16 (s, 2H), 3.89 (s, 3H) ppm. <sup>13</sup>C NMR (75.49 MHz, CDCl<sub>3</sub>): δ 189.00, 166.27, 160.43, 136.37, 135.68, 131.43, 130.32, 129.08, 128.57, 128.15, 128.06, 124.81, 120.86, 112.71, 69.48, 51.87 ppm. MS (ESI, SQ), *m/z* (%): 271.2 [M+H]<sup>+</sup>, 293.1 [M+Na]<sup>+</sup>.

#### 4.2.11. Methyl 3-((3-formylphenoxy)methyl)benzoate (25)

(white powder, yield 41%) <sup>1</sup>H NMR (300 MHz, CDCl<sub>3</sub>): δ 9.95 (s, 1H), 8.12 (s, 1H), 8.01 (d, *J* = 7.12 Hz, 1H), 7.63 (d, *J* = 7.12 Hz, 1H), 7.53–7.40 (m, 4H), 7.31–7.17 (m, 1H), 5.13 (s, 2H), 3.91 (s, 3H) ppm. <sup>13</sup>C NMR (75.49 MHz, CDCl<sub>3</sub>): δ 192.02, 166.76, 159.06, 137.83, 136.81, 131.86, 130.57, 130.19, 129.33, 128.77, 128.54, 123.86, 122.06, 113.25, 69.55, 52.21 ppm. MS (ESI, SQ), *m/z* (%): 271.2 [M+H]<sup>+</sup>, 293 [M+Na]<sup>+</sup>.

#### 4.2.12. Methyl 3-((4-formylphenoxy)methyl)benzoate (18)

The title compound was obtained starting from **28** and **30** (white powder, yield 51%) <sup>1</sup>H NMR (300 MHz, CDCl<sub>3</sub>): δ 9.83 (s, 1H), 8.09 (s, 1H), 7.98 (d, *J* = 7.56 Hz, 1H), 7.79 (d, *J* = 8.32 Hz, 2H), 7.60 (d, *J* = 7.56 Hz, 1H), 7.43 (t, *J* = 7.56 Hz, 1H), 7.04 (d, *J* = 8.32 Hz, 2H), 5.10 (s, 2H), 3.87 (s, 3H) ppm. <sup>13</sup>C NMR (75.49 MHz, CDCl<sub>3</sub>): δ 190.58, 166.50, 163.34, 136.53, 131.89, 131.81, 130.54, 130.23, 129.32, 128.76, 128.45, 115.05, 69.46, 52.10 ppm. MS (ESI, SQ), *m/z* (%): 271.2 [M+H]<sup>+</sup>, 293 [M+Na]<sup>+</sup>.

#### 4.2.13. Methyl 4-((2-tert-butyl-6-formylphenoxy)methyl)-2-fluorobenzoate (29)

(white powder, yield 50%, m.p. 70 °C) <sup>1</sup>H NMR (400 MHz, CDCl<sub>3</sub>): δ 10.26 (s, 1H), 8 (t, *J* = 7.77 Hz, 1H), 7.74 (dd, *J* = 7.63 Hz, *J* = 1.75 Hz, 1H), 7.65 (dd, *J* = 7.87 Hz, *J* = 1.75 Hz, 1H), 7.36 (d, *J* = 11.33 Hz, 1H), 7.32 (d, *J* = 8 Hz, 1H), 7.23 (t, *J* = 7.6 Hz, 1H), 5.08 (s, 2H), 3.95 (s, 3H), 1.43 (s, 9H) ppm. <sup>13</sup>C NMR (100.6 MHz, CDCl<sub>3</sub>): δ 189.98, 164.61 (d, *J* = 3.53 Hz), 162.13 (d, *J* = 261.3 Hz), 160.67, 144.05 (d, *J* = 8.61 Hz), 143.93, 133.8, 132.53, 129.91, 128.94, 124.54, 121.72 (d, *J* = 3.49 Hz), 118.06 (d, *J* = 10.17 Hz), 114.99 (d, *J* = 23.88 Hz), 78.06, 52.37, 35.27, 30.85 ppm. <sup>19</sup>F (376 MHz, CDCl<sub>3</sub>): δ -109.02 (dd, *J* = 11.33 Hz, *J* = 7.4 Hz) ppm. MS (APCI) found *m/z* 345.1497 (calcd for C<sub>20</sub>H<sub>21</sub>FO<sub>4</sub>: 345.1497 [M+Na]<sup>+</sup>).

#### 4.2.14. General procedure for the coupling of trioxotetrahydropyrimidin and the corresponding aldehydes to obtain: **1**, **2**, **3**, **4**, **10**, **11**, **12**, **13**, **19**, **20**, **21**, **26** and **30** [57]

The corresponding aldehydes (3.5 mmol), ethanol (10 mL), distilled water (10 mL), and barbituric acid (3 mmol) were refluxed overnight. The formed solids were collected by sucking filtration and washed with boiling water (3x15 mL), ethanol (3x15 mL), and ether (3x15 mL). The solids obtained were dried in vacuum.

#### 4.2.15. 8H-benzo[7,8]chromeno[2,3-d]pyrimidine-8,10(9H)-dione (1)

(orange powder, yield 46%, m.p. > 300 °C) <sup>1</sup>H NMR (600 MHz, DMSO-*d*<sub>6</sub>): δ 11.48 (s, 1H), 9.57 (s, 1H), 8.85 (d, *J* = 8.28 Hz, 1H), 8.51 (d, *J* = 9.45 Hz, 1H), 8.17 (d, *J* = 8.28 Hz, 1H), 7.86 (d, *J* = 9.45 Hz, 1H), 7.85 (t, *J* = 8.28 Hz, 1H), 7.74 (t, *J* = 8.28 Hz, 1H) ppm. <sup>13</sup>C NMR (150.9 MHz, DMSO-*d*<sub>6</sub>): δ 167.37, 161.20, 156.28, 154.27, 140.08, 138.20, 130.19, 129.59, 129.16, 129.04, 127.21, 122.98, 116.76, 114.51, 112.98 ppm. MS (ESI) found *m/z* 265.06097 (calcd for C<sub>15</sub>H<sub>8</sub>N<sub>2</sub>O<sub>3</sub>: 265.06077 [M+H]<sup>+</sup>). Anal. Calcd for C<sub>15</sub>H<sub>8</sub>N<sub>2</sub>O<sub>3</sub>: C, 68.18; H, 3.05; N, 10.60. Found: C, 68.18; H, 3.12; N, 11.01.

#### 4.2.16. 5-(3-acetylbenzylidene)pyrimidine-2,4,6(1H,3H,5H)-trione (2)

(yellow powder, yield 20%, m.p. 231 °C) <sup>1</sup>H NMR (300 MHz, DMSO-*d*<sub>6</sub>): δ 11.45 (s, 1H), 11.29 (s, 1H), 8.63 (s, 1H), 8.35 (s, 1H), 8.21 (s, 1H), 8.06 (d, *J* = 7.45 Hz, 1H), 7.61 (t, *J* = 7.45 Hz, 1H), 2.61 (s, 3H) ppm. <sup>13</sup>C NMR (75.49 MHz, DMSO-*d*<sub>6</sub>): δ 197.45, 163.05, 161.45, 153.38, 150.12, 136.74, 136.24, 133.11, 132.27, 130.80, 128.29, 120.13, 26.67 ppm. MS (ESI) found *m/z* 259.07166 (calcd for C<sub>13</sub>H<sub>10</sub>N<sub>2</sub>O<sub>4</sub>: 259.07133 [M+H]<sup>+</sup>). Anal. Calcd for C<sub>13</sub>H<sub>10</sub>N<sub>2</sub>O<sub>4</sub>: C, 60.47; H, 3.90; N, 10.85. Found: C, 60.54; H, 3.86; N, 10.83.

#### 4.2.17. 5-(3,4-dihydroxybenzylidene)pyrimidine-2,4,6(1H,3H,5H)-trione (3)

(orange powder, yield 46%, m.p. > 300 °C) <sup>1</sup>H NMR (600 MHz,

DMSO- $d_6$ ):  $\delta$  11.21 (s, 1H), 11.09 (s, 1H), 10.39 (bs, 1H), 9.46 (bs, 1H), 8.195 (d,  $J = 2.09$  Hz, 1H), 8.121 (s, 1H), 7.63 (dd,  $J = 8.51$  Hz,  $J = 2.09$  Hz, 1H), 6.86 (d,  $J = 8.51$  Hz, 1H) ppm.  $^{13}\text{C}$  NMR (150.9 MHz, DMSO- $d_6$ )  $\delta$  164.09, 162.14, 155.90, 152.25, 150.13, 144.74, 131.18, 124.16, 121.22, 115.26, 113.57 ppm. MS (ESI) found  $m/z$  249.05086 (calcd for  $\text{C}_{11}\text{H}_8\text{N}_2\text{O}_5$ : 249.05060  $[\text{M}+\text{H}]^+$ ). Anal. Calcd for  $\text{C}_{11}\text{H}_8\text{N}_2\text{O}_5$ : C, 53.23; H, 3.25; N, 11.29. Found: C, 53.45; H, 3.21; N, 11.81.

#### 4.2.18. 5-(anthracen-9-ylmethylene)pyrimidine-2,4,6-(1H,3H,5H)-trione (4)

(red powder, yield 54%, m.p.  $> 300^\circ\text{C}$ )  $^1\text{H}$  NMR (400 MHz, DMSO- $d_6$ ):  $\delta$  11.57 (s, 1H), 11.17 (s, 1H), 9.01 (s, 1H), 8.63 (s, 1H), 8.12 (s, 2H), 7.97 (s, 2H), 7.52 (s, 4H) ppm.  $^{13}\text{C}$  NMR (75.46 MHz, DMSO- $d_6$ )  $\delta$  162.28, 160.41, 151.20, 150.42, 130.50, 129.38, 128.57, 127.69, 127.55, 126.12, 125.42 ppm. MS (ESI) found  $m/z$  317.009259 (calcd for  $\text{C}_{19}\text{H}_{12}\text{N}_2\text{O}_3$ : 317.09207  $[\text{M}+\text{H}]^+$ ). Anal. Calcd for  $\text{C}_{19}\text{H}_{12}\text{N}_2\text{O}_3$ : C, 72.15; H, 3.82; N, 8.86. Found: C, 72.12; H, 3.79; N, 8.72.

#### 4.2.19. Methyl 4-((2-((2,4,6-trioxotetrahydropyrimidin-5(2H)-ylidene)methyl)phenoxy)methyl)benzoate (10)

(yellow powder, yield 64%)  $^1\text{H}$  NMR (300 MHz, DMSO- $d_6$ ):  $\delta$  11.35 (s, 1H), 11.17 (s, 1H), 8.58 (s, 1H), 8.06–7.93 (m, 3H), 7.60 (d,  $J = 8.28$  Hz, 2H), 7.50 (t,  $J = 7.29$  Hz, 1H), 7.16 (d,  $J = 8.28$  Hz, 1H), 7.01 (t,  $J = 7.62$  Hz, 1H), 5.34 (s, 2H), 3.86 (s, 3H) ppm.  $^{13}\text{C}$  NMR (150.9 MHz, DMSO- $d_6$ ):  $\delta$  165.87, 163.22, 161.32, 157.64, 150.14, 149.65, 142.05, 133.71, 132.40, 129.28, 129.06, 127.32, 122.07, 119.93, 118.94, 112.39, 69.25, 52.06 ppm. MS (ESI, SQ),  $m/z$  (%): 381.3  $[\text{M}+\text{H}]^+$ .

#### 4.2.20. Methyl 4-((3-((2,4,6-trioxotetrahydropyrimidin-5(2H)-ylidene)methyl)phenoxy)methyl)benzoate (11)

(yellow powder, yield 57%, m.p.  $256^\circ\text{C}$ )  $^1\text{H}$  NMR (300 MHz, DMSO- $d_6$ ):  $\delta$  11.41 (s, 1H), 11.26 (s, 1H), 8.25 (s, 1H), 7.99 (d,  $J = 7.84$  Hz, 2H), 7.91 (s, 1H), 7.71–7.57 (m, 3H), 7.405 (t,  $J = 8.10$  Hz, 1H), 7.22 (d,  $J = 8.10$  Hz, 1H), 5.25 (s, 2H), 3.86 (s, 3H) ppm.  $^{13}\text{C}$  NMR (75.49 MHz, DMSO- $d_6$ ):  $\delta$  165.93, 163.27, 161.49, 157.43, 154.19, 150.07, 142.26, 133.84, 129.27, 129.12, 128.95, 127.47, 126.29, 119.32, 118.93, 118.6468.62, 52.06 ppm. MS (ESI) found  $m/z$  403.09000 (calcd for  $\text{C}_{20}\text{H}_{16}\text{N}_2\text{O}_6$ : 403.09006  $[\text{M}+\text{Na}]^+$ ). Anal. Calcd for  $\text{C}_{20}\text{H}_{16}\text{N}_2\text{O}_6$ : C, 63.16; H, 4.24; N, 7.37. Found: C, 63.23; H, 4.35; N, 7.56.

#### 4.2.21. Methyl 4-((2-(tert-butyl)-6-((2,4,6-trioxotetrahydropyrimidin-5(2H)-ylidene)methyl)phenoxy)methyl)benzoate (12)

(yellow powder, yield 14%, m.p.  $184^\circ\text{C}$ )  $^1\text{H}$  NMR (300 MHz, DMSO- $d_6$ ):  $\delta$  11.33 (s, 1H), 11.19 (s, 1H), 8.34 (s, 1H), 7.99 (d,  $J = 8.08$  Hz, 2H), 7.70 (d,  $J = 7.85$  Hz, 1H), 7.61 (d,  $J = 8.08$  Hz, 2H), 7.48 (d,  $J = 7.85$  Hz, 1H), 7.12 (t,  $J = 7.85$  Hz, 1H), 4.94 (s, 2H), 3.94 (s, 3H), 1.38 (s, 9H) ppm.  $^{13}\text{C}$  NMR (100.6 MHz, DMSO- $d_6$ ):  $\delta$  165.88, 162.95, 161.14, 157.91, 150.35, 150.20, 142.04, 141.62, 130.30, 130.27, 129.21, 129.05, 127.75, 127.37, 122.78, 119.60, 76.96, 52.07, 34.64, 30.50 ppm. MS (ESI) found  $m/z$  437.17087 (calcd for  $\text{C}_{24}\text{H}_{24}\text{N}_2\text{O}_6$ : 437.17071  $[\text{M}+\text{H}]^+$ ). Anal. Calcd for  $\text{C}_{24}\text{H}_{24}\text{N}_2\text{O}_6$ : C, 66.05; H, 5.54; N, 6.42. Found: C, 66.12; H, 5.53; N, 6.81.

#### 4.2.22. Methyl 4-((2,6-dimethyl-4-((2,4,6-trioxotetrahydropyrimidin-5(2H)-ylidene)methyl)phenoxy)methyl)benzoate (13)

(yellow powder, yield 73%, m.p.  $281^\circ\text{C}$ )  $^1\text{H}$  NMR (400 MHz, DMSO- $d_6$ ):  $\delta$  11.35 (s, 1H), 11.20 (s, 1H), 8.19 (s, 1H), 8.02 (d,  $J = 8.26$  Hz, 2H), 7.99 (s, 2H), 7.66 (d,  $J = 8.26$  Hz, 2H), 5.00 (s, 2H), 3.87 (s, 3H), 2.97 (s, 6H) ppm.  $^{13}\text{C}$  NMR (100.6 MHz, DMSO- $d_6$ ):  $\delta$  165.94, 163.54, 161.69, 159.16, 154.52, 150.11, 142.49, 135.17, 130.44, 129.24, 129.09, 128.26, 127.80, 117.32, 72.68, 52.07, 16.14 ppm. MS (ESI) found  $m/z$  409.13950 (calcd for  $\text{C}_{22}\text{H}_{20}\text{N}_2\text{O}_6$ :

409.13941  $[\text{M}+\text{H}]^+$ ). Anal. Calcd for  $\text{C}_{22}\text{H}_{20}\text{N}_2\text{O}_6$ : C, 64.70; H, 4.94; N, 6.86. Found: C, 65.03; H, 4.76; N, 6.77.

#### 4.2.23. Methyl 3-((2-methyl-6-((2,4,6-trioxotetrahydropyrimidin-5(2H)-ylidene)methyl)phenoxy)methyl)benzoate (19)

(yellow powder, yield 46%, m.p.  $198^\circ\text{C}$ )  $^1\text{H}$ -NMR (600 MHz, DMSO- $d_6$ ):  $\delta$  11.31 (s, 1H), 11.12 (s, 1H), 8.33 (s, 1H), 7.97 (s, 1H), 7.91 (d,  $J = 7.81$  Hz, 1H), 7.76 (d,  $J = 7.81$  Hz, 1H), 7.65 (d,  $J = 7.51$  Hz, 1H), 7.49 (t,  $J = 7.81$  Hz, 1H), 7.40 (d,  $J = 7.51$  Hz, 1H), 7.71 (t,  $J = 7.51$  Hz, 1H) ppm.  $^{13}\text{C}$  NMR (150.9 MHz, DMSO- $d_6$ ):  $\delta$  165.92, 162.98, 161.05, 156.62, 150.35, 150.21, 137.22, 134.71, 133.42, 130.73, 129.92, 129.84, 129.93, 128.90, 127.35, 123.25, 119.47, 75.37, 52.18, 15.85 ppm. MS (ESI) found  $m/z$  395.12393 (calcd for  $\text{C}_{21}\text{H}_{18}\text{N}_2\text{O}_6$ : 395.12376  $[\text{M}+\text{H}]^+$ ). Anal. Calcd for  $\text{C}_{21}\text{H}_{18}\text{N}_2\text{O}_6$ : C, 63.96; H, 4.60; N, 7.10. Found: C, 63.45; H, 4.55; N, 7.01.

#### 4.2.24. Methyl 3-((2-((2,4,6-trioxotetrahydropyrimidin-5(2H)-ylidene)methyl)phenoxy)methyl)benzoate (20)

(orange powder, yield 56%, m.p.  $200^\circ\text{C}$ )  $^1\text{H}$  NMR (300 MHz, DMSO- $d_6$ ):  $\delta$  11.46 (s, 1H), 11.27 (s, 1H), 8.68 (s, 1H), 8.17 (s, 1H), 8.10 (d,  $J = 8.21$  Hz, 1H), 8.04 (d,  $J = 7.62$  Hz, 1H), 7.85 (d,  $J = 7.33$  Hz, 1H), 7.68 (t,  $J = 7.59$  Hz, 1H), 7.61 (t,  $J = 7.87$  Hz, 1H), 7.31 (d,  $J = 8.50$  Hz, 1H), 7.116 (t,  $J = 7.62$  Hz, 1H) ppm.  $^{13}\text{C}$  NMR (75.49 MHz, DMSO- $d_6$ ):  $\delta$  165.90, 163.18, 161.30, 157.66, 150.15, 149.72, 137.38, 133.70, 132.38, 132.04, 129.81, 128.96, 128.59, 127.88, 122.08, 119.87, 118.92, 112.41, 69.20, 52.12 ppm. MS (ESI) found  $m/z$  381.10834 (calcd for  $\text{C}_{20}\text{H}_{16}\text{N}_2\text{O}_6$ : 381.10811  $[\text{M}+\text{H}]^+$ ). Anal. Calcd for  $\text{C}_{20}\text{H}_{16}\text{N}_2\text{O}_6$ : C, 63.16; H, 4.24; N, 7.37. Found: C, 63.16; H, 4.32; N, 7.12.

#### 4.2.25. Methyl 3-((4-((2,4,6-trioxotetrahydropyrimidin-5(2H)-ylidene)methyl)phenoxy)methyl)benzoate (21)

The title compound was obtained starting from 34 and 5 (yellow powder, yield 71%, m.p.  $227^\circ\text{C}$ )  $^1\text{H}$  NMR (300 MHz, DMSO- $d_6$ ):  $\delta$  11.33 (s, 1H), 11.20 (s, 1H), 8.37 (d,  $J = 8.34$  Hz, 2H), 8.26 (s, 1H), 7.95 (d,  $J = 7.47$  Hz, 1H), 7.77 (d,  $J = 7.60$  Hz, 1H), 7.58 (t,  $J = 7.60$  Hz, 1H), 7.16 (d,  $J = 8.34$  Hz, 2H), 5.34 (s, 2H), 3.87 (s, 3H) ppm.  $^{13}\text{C}$  NMR (75.45 MHz, DMSO- $d_6$ ):  $\delta$  165.93, 163.798, 162.18, 162.06, 154.74, 150.12, 137.31, 137.14, 132.46, 129.83, 128.99, 128.72, 128.22, 125.40, 115.71, 114.60, 68.88, 52.14 ppm. MS (ESI) found  $m/z$  381.10818 (calcd for  $\text{C}_{20}\text{H}_{16}\text{N}_2\text{O}_6$ : 381.10811  $[\text{M}+\text{H}]^+$ ). Anal. Calcd for  $\text{C}_{20}\text{H}_{16}\text{N}_2\text{O}_6$ : C, 63.16; H, 4.24; N, 7.37. Found: C, 62.39; H, 4.63; N, 7.24.

#### 4.2.26. Methyl 3-((3-((2,4,6-trioxotetrahydropyrimidin-5(2H)-ylidene)methyl)phenoxy)methyl)benzoate (26)

The title compound was obtained starting from 33 and 5 (yellow powder, yield 17%, m.p.  $158^\circ\text{C}$ )  $^1\text{H}$  NMR (300 MHz, DMSO- $d_6$ ):  $\delta$  11.40 (s, 1H), 11.25 (s, 1H), 8.25 (s, 1H), 8.06 (s, 1H), 7.93–7.83 (m, 2H), 7.75 (d,  $J = 7.54$  Hz, 1H), 7.66 (d,  $J = 7.95$  Hz, 1H), 7.57 (t,  $J = 7.54$  Hz, 1H), 7.41 (t,  $J = 7.95$  Hz, 1H), 7.22 (d,  $J = 8.37$  Hz, 1H), 5.24 (s, 2H), 3.87 (s, 3H) ppm.  $^{13}\text{C}$  NMR (150.9 MHz, DMSO- $d_6$ ):  $\delta$  165.96, 163.26, 161.48, 157.49, 154.24, 150.05, 137.57, 133.85, 132.32, 129.79, 129.11, 128.94, 128.55, 128.06, 126.19, 119.32, 118.89, 118.73, 68.67, 52.11 ppm. MS (ESI) found  $m/z$  381.10840 (calcd for  $\text{C}_{20}\text{H}_{16}\text{N}_2\text{O}_6$ : 381.10811  $[\text{M}+\text{H}]^+$ ). Anal. Calcd for  $\text{C}_{20}\text{H}_{16}\text{N}_2\text{O}_6$ : C, 63.16; H, 4.24; N, 7.37. Found: C, 63.19; H, 4.29; N, 7.14.

#### 4.2.27. Methyl 4-((2-(tert-butyl)-6-((2,4,6-trioxotetrahydropyrimidin-5(2H)-ylidene)methyl)phenoxy)methyl)-2-fluorobenzoate (30)

(yellow powder, yield 39%, m.p.  $210^\circ\text{C}$ )  $^1\text{H}$  NMR (400 MHz, DMSO- $d_6$ ):  $\delta$  11.31 (s, 1H), 11.18 (s, 1H), 8.31 (s, 1H), 7.93 (t,  $J = 7.61$  Hz, 1H), 7.68 (d,  $J = 7.51$  Hz, 1H), 7.47 (d,  $J = 6.85$  Hz, 1H), 7.42 (d,  $J = 7.71$  Hz, 1H), 7.41 (d,  $J = 11.98$  Hz, 1H), 7.12 (t,  $J = 7.81$  Hz, 1H), 4.93 (s, 2H), 3.87 (s, 3H), 1.37 (s, 9H) ppm.  $^{13}\text{C}$  NMR

(100.6 MHz, DMSO- $d_6$ ):  $\delta$  163.64 (d,  $J$  = 3.08 Hz), 162.9, 161.09, 160.8 (d,  $J$  = 257.47 Hz), 159.51, 157.62, 150.178, 150.102, 144.66 (d,  $J$  = 8.52 Hz), 141.58, 131.89, 130.23, 130.23, 127.71, 122.87, 119.77, 117.28 (d,  $J$  = 10.43 Hz), 115.35 (d,  $J$  = 23.26 Hz), 76, 52.27, 34.62, 30.52 ppm.  $^{19}\text{F}$  (376 MHz, DMSO- $d_6$ ):  $\delta$  -110.47 (dd,  $J$  = 11.98 Hz,  $J$  = 7.52 Hz) ppm. MS (ESI) found  $m/z$  455.1621 (calcd for  $\text{C}_{24}\text{H}_{23}\text{FN}_2\text{O}_6$ : 455.1613  $[\text{M} + \text{H}]^+$ ).

#### 4.2.28. General procedure for the synthesis of benzoic acid derivatives: **14**, **22**, **23**, **24** [42]

To a stirred solution of **10**, **19**, **20**, and **21** (5.55 mmol) in 1,4-dioxane/methanol/water (1:1:1) (30 mL), 2 M NaOH (5.55 mL, 11.10 mmol) was added dropwise. After 5 h the mixture was acidified to pH 3 with 1 M HCl, the organic phase was evaporated, the residue was dissolved in ethyl acetate (50 mL), washed with 10% citric acid (2x20 mL) and brine (2x15 mL), dried over  $\text{Na}_2\text{SO}_4$ , and concentrated under reduced pressure.

#### 4.2.29. 4-((2-((2,4,6-trioxotetrahydropyrimidin-5(2H) ylidene) methyl) phenoxy) methyl) benzoic acid (**14**)

(yellow powder, yield 53%)  $^1\text{H}$  NMR (600 MHz, DMSO- $d_6$ ):  $\delta$  12.97 (bs, 1H), 11.33 (s, 1H), 11.16 (s, 1H), 8.58 (s, 1H), 8.05 (d,  $J$  = 8.79 Hz, 1H), 7.97 (d,  $J$  = 8.44 Hz, 2H), 7.57 (d,  $J$  = 8.44 Hz, 2H), 7.49 (t,  $J$  = 8.79 Hz, 1H), 7.17 (d,  $J$  = 8.79 Hz, 1H), 7.00 (t,  $J$  = 8.79 Hz, 1H) ppm.  $^{13}\text{C}$  NMR (150.9 MHz, DMSO- $d_6$ ):  $\delta$  166.91, 163.23, 161.32, 157.67, 150.14, 149.65, 141.55, 133.71, 132.40, 130.40, 129.41, 127.16, 122.03, 119.88, 118.92, 112.35, 69.28 ppm. MS (ESI, SQ),  $m/z$  (%): (389.1)  $[\text{M} + \text{Na}]^+$ .

#### 4.2.30. 3-((2-methyl-6-((2,4,6-trioxotetrahydropyrimidin-5(2H)-ylidene) methyl)phenoxy) methyl) benzoic acid (**22**)

(yellow powder, yield 59%, m.p. 234 °C)  $^1\text{H}$  NMR (600 MHz, DMSO- $d_6$ ):  $\delta$  11.32 (s, 1H), 11.14 (s, 1H), 8.39 (s, 1H), 7.98 (s, 1H), 7.91 (d,  $J$  = 7.82 Hz, 1H), 7.79 (d,  $J$  = 7.82 Hz, 1H), 7.65 (d,  $J$  = 7.41 Hz, 1H), 7.49 (d,  $J$  = 7.82 Hz, 1H), 7.41 (d,  $J$  = 7.41 Hz, 1H), 7.10 (t,  $J$  = 7.41 Hz, 1H), 4.90 (s, 2H), 2.30 (s, 3H) ppm.  $^{13}\text{C}$  NMR (150.9 MHz, DMSO- $d_6$ ):  $\delta$  166.91, 162.98, 161.06, 156.66, 150.15, 136.98, 134.65, 132.78, 130.88, 130.64, 129.88, 129.16, 128.98, 128.61, 127.12, 123.17, 119.52, 75.48, 15.74 ppm. MS (ESI) found  $m/z$  403.09021 (calcd for  $\text{C}_{20}\text{H}_{16}\text{N}_2\text{O}_6$ : 403.09006  $[\text{M} + \text{Na}]^+$ ).

#### 4.2.31. 3-((2-((2,4,6-trioxotetrahydropyrimidin-5(2H) ylidene) methyl) phenoxy) methyl) benzoic acid (**23**)

(yellow powder, yield 49%, m.p. 242 °C)  $^1\text{H}$  NMR (600 MHz, DMSO- $d_6$ ):  $\delta$  11.31 (s, 1H), 11.13 (s, 1H), 8.55 (s, 1H), 8.2 (s, 1H), 7.99 (d,  $J$  = 8.05 Hz, 1H), 7.91 (d,  $J$  = 7.47 Hz, 1H), 7.71 (d,  $J$  = 8.05 Hz, 1H), 7.54 (t,  $J$  = 8.05 Hz, 1H), 7.50 (t,  $J$  = 7.47 Hz, 1H), 7.19 (d,  $J$  = 8.38 Hz, 1H), 7.00 (t,  $J$  = 7.47 Hz, 1H) ppm.  $^{13}\text{C}$  NMR (150.9 MHz, DMSO- $d_6$ ):  $\delta$  167.00, 163.25, 161.36, 157.81, 150.18, 149.75, 137.18, 133.80, 132.49, 131.76, 131.03, 128.84, 128.26, 122.06, 119.87, 118.90, 112.46, 69.44 ppm. MS (ESI) found  $m/z$  367.09259. calcd for  $\text{C}_{19}\text{H}_{14}\text{N}_2\text{O}_6$ : 367.09246  $[\text{M} + \text{H}]^+$ . Anal. Calcd for  $\text{C}_{19}\text{H}_{14}\text{N}_2\text{O}_6$ : C, 62.30; H, 3.85; N, 7.65. Found: C, 62.32; H, 3.90; N, 7.58.

#### 4.2.32. 3-((4-((2,4,6-trioxotetrahydropyrimidin - 5(2H) ylidene) methyl) phenoxy) methyl) benzoic acid (**24**)

(yellow powder, yield 61%, m.p. 289 °C)  $^1\text{H}$  NMR (600 MHz, DMSO- $d_6$ ):  $\delta$  11.30 (s, 1H), 11.17 (s, 1H), 8.37 (d,  $J$  = 9 Hz, 2H), 8.26 (s, 1H), 7.93 (d,  $J$  = 7.79 Hz, 1H), 7.73 (d,  $J$  = 7.79 Hz, 1H), 7.55 (t,  $J$  = 7.79 Hz, 1H), 7.16 (d,  $J$  = 9 Hz, 2H), 5.33 (s, 2H), 2.09 (s, 3H) ppm.  $^{13}\text{C}$  NMR (150.9 MHz, DMSO- $d_6$ ):  $\delta$  166.98, 163.77, 162.22, 162.03, 154.74, 150.08, 137.28, 136.90, 132.01, 130.99, 128.85, 128.79, 128.38, 125.38, 115.71, 114.61, 68.99 ppm. MS (ESI) found  $m/z$  367.09265 (calcd for  $\text{C}_{19}\text{H}_{14}\text{N}_2\text{O}_6$ : 367.09246  $[\text{M} + \text{H}]^+$ ). Anal. Calcd for  $\text{C}_{19}\text{H}_{14}\text{N}_2\text{O}_6$ : C, 62.30; H, 3.85; N, 7.65. Found: C, 62.12; H, 3.91; N, 7.43.

### 4.3. Biological part

#### 4.3.1. In vitro human leukocyte trafficking assays.

Leukocyte trafficking assays were conducted as described previously [75,76]. Briefly, human umbilical vein endothelial cells (HUVECs) were isolated by collagenase treatment of umbilical veins and maintained (passages 2–4) in Medium 199 containing 10% FCS, 15  $\mu\text{g}/\text{mL}$  endothelial cell growth supplement (Upstate Biotechnology), 100  $\mu\text{g}/\text{mL}$  heparin, and 50  $\mu\text{M}$  hydrocortisone. For the flow assays, HUVECs were cultured after maximum of 3–5 passages in chamber slides (m-slide VI 0.1 ibiTreat, IBIDI), previously coated with 0.2% gelatin [76–78] (Sigma-Aldrich) and 1  $\text{mg}/\text{mL}$  Collagen G (Biochrom AG) for 2–3 days and then treated for 24 h with acute or chronic inflammation protocols using tumor necrosis factor  $\alpha$  (TNF- $\alpha$ ) at 1000 U/mL alone or in combination with interferon  $\gamma$  (IFN  $\gamma$ ), at 500 U/mL for chronic inflammatory protocols. The compounds to be tested and leukocytes were added at 30  $\mu\text{M}$  (Supporting Information Fig. S1A). Monocytes, T lymphocytes, and B lymphocytes were purified from EDTA blood collected from healthy donors using Ficoll gradients and negative selection kits (Miltenyi Biotec) for those types of cells. The slides containing the cultured HUVEC monolayers were then mounted to a flow system set at 37 °C and flow was generated over the HUVEC monolayer by perfusing a wash medium or a medium containing the leukocyte suspension using a calibrated pump (Supporting Information Fig. S1B). The flow rate, expressed as a measurement of shear stress, was representative of small venules/capillaries (0.05 Pascal (Pa)). The first stage of the assay was a washing procedure, where the wash buffer was perfused over the HUVECs for 10 min (Supporting Information Fig. S1C, step 1). For chronic activation protocols, an additional flow step of 15 min with wash buffer containing 1  $\mu\text{M}$  of CXCL12 for T cell assays and 1  $\mu\text{M}$  CXCL13 for B cell assays. Wash buffer was then perfused over the HUVECs for 10 min to remove unbound chemokine, before purified leukocytes were perfused over the HUVECs for 5 min (Supporting Information Fig. S1C, step 2), followed by 45 min with wash buffer (Supporting Information Fig. S1C, step 3). Throughout steps 2–3, images of the captured leukocytes under flow are made using phase-contrast microscopy, and a high-resolution camera. Individual images are recorded every 30 s and compiled into movie sequences, allowing analysis of individual leukocytes over large areas. Leukocytes adherent to the surface of the HUVECs have a phase-white appearance, whereas those that have transmigrated have a phase-black appearance. For individual cell tracking, the phase appearance of each leukocyte was marked at 1-minute intervals in defined areas by running the movies forth and back multiple times [44].

Adhesion events were recorded as the total number of cells per unit field ( $\text{mm}^2$ ). Transmigration events are presented as a percentage of total leukocytes captured from flow per unit field. All experiments were carried out using triplicate fields and are presented as a mean value with + standard error measurements (+SEM). Statistical analyses assume parametric distributions, and are conducted using Student's  $t$ -test.  $P$  values from significance scores are presented in the figures as follows: \*  $P$  < 0.05, \*\*  $P$  < 0.01, \*\*\*  $P$  < 0.005 [44].

#### 4.4. Cell cultures

Jeko-1 and PC12 cells were grown in RPMI 1640 medium (11.1 mM glucose) supplemented with 10% FCS, 1% glutamine, and antibiotics (100  $\mu\text{g}/\text{mL}$  penicillin, 100  $\mu\text{g}/\text{mL}$  streptomycin) at 37 °C in a 5%  $\text{CO}_2$  humidified atmosphere. HeLa cells were grown in DMEM, 22.5 mM glucose, 10% FCS, 1% glutamine, and antibiotics (100  $\mu\text{g}/\text{mL}$  penicillin, 100  $\mu\text{g}/\text{mL}$  streptomycin) at 37 °C in a 5%  $\text{CO}_2$  humidified atmosphere.

#### 4.5. Cell lysate preparation.

##### 4.5.1. Lysis of suspension culture (Jeko-1 cell line)

Cells were grown to a density of 2 million cells/mL. Thereafter, cells were centrifuged (300g for 5 min) in a conical tube for 5 min at room

temperature. The obtained pellet was washed with 10 mL of ice cold PBS and then spun for an additional time (300g for 5 min). PBS was aspirated from the tube supernatant. RIPA Lysis buffer (50  $\mu$ L) with protease inhibitor mix was added per  $1 \times 10^6$  cells. The lysates were kept on ice for 15 min and then sonicated by Branson Digital Sonifier® set at 50% amplitude) three times for two seconds, each with at least a 1 min rest on ice between each two-second pulse. Thereafter, the lysates were incubated for an additional 15 min on ice and centrifuged at 13,000g for 5 min at 4 °C. The protein concentration was determined by the bicinchoninic acid method. Aliquots were stored at  $-20$  °C.

#### 4.5.2. Lysis to adherent cells (HeLa cell line)

HeLa cells were grown to approximately 80% confluence. After the medium was aspirated, the dishes were kept on ice for all the lysis preparation steps. Cells were washed one time with 10 mL of ice cold PBS. An excess of PBS was aspirated. Then 500  $\mu$ L of RIPA lysis buffer with protease inhibitor mix was added to each plate and the buffer was swirled very well for an equal distribution of the buffer. Afterwards, cell scraper cells were scraped and transferred to a 15 mL test tube. The obtained lysates were incubated on ice for 15 min and sonicated by Branson Digital Sonifier (at 50% amplitude) three times for two seconds each with at least 1 min rest on ice between each two-second pulse. Thereafter, the lysates were centrifuged at 13,000g for 5 min at 4 °C. The supernatant was collected into new microtubes. The protein concentration was determined by the bicinchoninic acid method. Aliquots were stored at  $-20$  °C.

#### 4.6. Determination of MAdCAM-1 binding affinity in the presence of compound 12 by the EIAab® ELISA kit

This immunoassay kit allows for the *in vitro* quantitative determination of human hMAdCAM-1 concentrations in serum, plasma, tissue homogenates, and cell culture supernates. The plate provided in this kit was pre-coated with an antibody specific to hMAdCAM-1. HeLa cell lysates (50  $\mu$ g of total protein) were placed in each well. The lysates were incubated with compound 12 or DMSO on ice with gentle shaking for 30 min. Thereafter, the samples were treated with kit reagents and processed according to the kit manufacturer's instructions. Finally, the optical density of each well was detected using a micro plate reader at 450 nm.

#### 4.7. Determination of JAM-C binding affinity in the presence of compound 12 by the RayBio® human JAM-C ELISA kit

Jeko-1 cell lysates were used for the assay. First, 50  $\mu$ g of total protein was placed in each well. The lysates were incubated with compound 12 or DMSO on ice with gentle shaking for 30 min. The RayBio® Human JAM-C ELISA kit was used for determining the possible inhibitory effect of compound 12 on JAM-C binding. This assay employs an antibody specific for human JAM-C coated on a 96-well plate. After the pre-incubation with compound 12, lysates were processed according to the kit manufacturer's instructions. Finally, the optical density of each well was detected using a micro plate reader at 450 nm.

#### 4.8. Determination of VCAM-1 binding affinity in the presence of compound 12 by the human VCAM-1 ELISA Kit

The assay was conducted as we described above (MAdCAM-1 assay).

#### 4.9. Determination of $\beta$ integrins mediated Jaco-1 cell adhesion in the presence of compound 12 by the $\beta$ Integrin-Mediated cell adhesion Kit

The assay was conducted as we described in manufacturer protocol for dispersed cells.

#### 4.10. $^{19}$ FNMR of compound 30 in HeLa and PC12 cells lysates

Cells were cultured as described above in Petri dishes. Compound 30 (2 mg in 100  $\mu$ L of DMSO) was introduced into the medium (12 mL) Control cells received only 100  $\mu$ L of DMSO. The cells were incubated for 30 min. The medium was taking out by vacuum aspiration. The cells were washed with PBS (room temperature) 10 mL  $\times$  3 times. The cells were lysed with hypertonic lysis buffer (0.1 M, Tris, pH = 8.8; 0.15 M, NaCl, 0.25% SDS in water, 200  $\mu$ L per plate). The obtained lysates were centrifuged in 13,500 rpm for 20 min at 4 °C. The obtained lysates were taken into NMR tubes. The 300  $\mu$ L of D<sub>2</sub>O were added to each tube and  $^{19}$ FNMR measurements were conducted.

#### 4.11. Methylcellulose-based suspension

1% methyl cellulose in double distilled water (DDW) solution was prepared by adding 0.5 g methyl cellulose into 50 mL of DDW and stirring the solution at the lowest possible speed (without making bubbles) overnight at room temperature. Compound 12 stock solution was prepared at a concentration of 20 mg/mL at room temperature following an established protocol: First, 30 mg of the compound were placed in a glass vial together with a small magnet. Thereafter, 1.5 mL of 1% methylcellulose were added by very slow circular swirling movements. The entire surface of the vial was gently covered by the solvent and powder was not allowed to float above the liquid. The resulting suspension was stirred at the lowest possible speed up to 48 h at room temperature. An intermediate stock solution of compound 12 at a 10 mg/mL concentration was prepared by diluting the obtained stock solution (adding the stock solution directly to equal amounts of DDW). The obtained stock solution was stirred at the lowest possible speed for another hour at room temperature. Finally, a compound 12 working solution at 3 mg/mL was prepared by diluting an intermediate stock solution (v/v) with DDW accordingly. The working solution of compound 12 (gentle suspension) was stirred at a low speed ( $\sim$ 80–100 rpm) for 30 min – 1 h prior to use in the animal experiments. The working solution of the compound (3 mg/mL) was prepared on the day that the experiment starts. Compound 12 is stable for at least 7 days at a 10 mg/mL concentration, while constantly being stirred at room temperature.

#### 4.12. Animals

Mice were handled according to the regulations formulated by the Israel Animal Care and Use Committee (Ministry of Health) and the University Medical Center, University of Geneva (Geneva, Switzerland). All experiments were approved by the Animal Care Committee of Geneva and by the Swiss National Veterinary Law. In Israel all experiments were approved by the Animal Care Committee of the Ministry of Health.

#### 4.13. Acute toxicology

Eight experimental groups with 5 female 6–7-week-old C57BL mice each and one control group were used for the experiment. Mice were injected using compound 12 or a suitable control using a methylcellulose formulation. Mice from all experimental groups were observed for a possible change in their behavior: immediately post-dosing and following 2 h post-administration. Mice from all groups were euthanized with isoflurane 24 h after the last administered dose. Sampling for WBC and White Blood Differentiation: 200  $\mu$ L of whole blood were collected into EDTA tubes (Greiner MiniCollect K3EDTA tubes). The remaining whole blood (300–400  $\mu$ L) was collected for serum preparation (Greiner MiniCollect Z Serum Tubes). All blood tests were conducted in American Medical Labs, Herzliyah, Israel. Liver, spleen, lungs, heart, and kidneys were collected from each mouse and placed into vials with 4% buffered formalin for future preparation of paraffin blocks. Sections

from each organ of each animal were stained with H&E and histological evaluation of the tissue was performed for identification of macrosigns of possible toxicity.

#### 4.14. Chronic toxicology (GLP guided experiment)

The experiment was conducted by the “Science and Action” company according to GLP protocol. The data and detailed protocol are presented in the SI.

#### 4.15. IBD mouse model

Female 7–8-week-old C57BL mice were treated with 1.5% dextran sodium sulfate in drinking water. Compound **12** was administered as described. Determination of the individual body weights of animals was made prior to each dosing and the administered volume was adjusted. During the administration of the test compound, the mouse body weights were measured daily. The DAI score was monitored daily, according to criteria mentioned in Table 1. Mice from all groups were euthanized with isoflurane 24 h after administering the last dose. The colon was collected from each mouse from all groups, filled with 4% buffered formalin, and the colon length was measured.

#### 4.16. MS mouse model

Female 7–8-week-old C57BL mice were treated with OG35-55/CFA according to the standard protocol [79]. After the onset of EAE, mice were assigned to the groups (treated and untreated as described). The body weight of animals was determined prior to starting the experiment and the administered volume of the formulation of compound **12** was adjusted according to the body weight during the experiment; the body weight was measured daily. The severity of the EAE score was monitored daily, according to criteria mentioned in Table 2. Mice from all groups were euthanized with isoflurane 24 h after the last administered dose.

#### 4.17. The High-Fat Diet-Induced NAFLD mouse model.

C57BL/6 male mice were fed ad libitum a high-fat diet, no high-carbohydrate diet (modified western diet, WD) with 42% kcal from fat containing 0.1% cholesterol (Harlan TD.88137) with normal water (without high fructose-glucose solution) for 14 weeks prior to initiating the treatment. Control mice were fed a standard chow diet (CD, Harlan TD.7012) with normal water (NW). A working formulation of compound **12** was administered on the 85th day of the high-fat diet (15 mg/kg, for SC and IP using a 30 mg/kg q3w regimen for PO along with a qd regimen) to a mock-treated (vehicle) control group by IP injections at the same volume and regimen as a correspondingly treated group for 65 days. The body weight of animals was determined prior to initiating the treatment and the administered volume of compound **12** was adjusted according to the body weight. All animals were euthanized 24 h after the last administered dose. At necropsy, liver and mesenteric fat wet weights were determined. Liver and mesenteric fat were fixed with 4% buffered formalin, embedded in paraffin sections, and H&E stained. Steatohepatitis was defined by the presence of steatosis, inflammation, and hepatocellular ballooning, according to the fatty liver inhibition of progression (FLIP) algorithm. The severities of steatosis, lobular inflammation, and hepatocellular ballooning were scored using the NASH-Clinical Research Network (CRN) criteria. The NAFLD activity score (NAS) was calculated by adding the scores of steatosis (the maximum score was 3). It is defined by more than 66% of hepatocytes containing fat droplets; lobular inflammation (the maximum score of 3) is defined by > 4 foci/200 field; hepatocyte ballooning (the maximum score of 2) is defined by many cells or prominent ballooning. Ordinary one-way ANOVA statistical analysis was performed.

#### 4.18. Collagen-Induced arthritis (CIA) model in DBA/1 Mice

Male DBA/1 mice (7–8 weeks of age) were injected with CII (Type II collagen) + CFA (complete Freund's adjuvant) emulsion on day 0 (SC) to stimulate CIA [80]. On day 21, the animals received the same amount of the emulsion as a booster. Twice between days 0 and 18 after immunization (before enrollment begins), both hind paws of all mice were measured using calipers to establish the baseline values for paw thickness. On day 22 the mice were enrolled into groups when they first exhibited paw swelling and treatment was initiated. A compound **12** was administered by IP injections at 15 mg/kg dose using the q3w regimen. The mock-treated (vehicle) control group was administered IP with the same volume and regimen as the treatment group. Administration was performed at a constant volume dosage based on individual body weight. The severity of CIA was monitored daily. The CIA scoring is on a scale of 0 to 16 (0 to 4 for each paw, adding the scores for all 4 paws). On day 43 (24 h after the last administered dose), all paw thicknesses were measured and the mice were euthanized. All limbs from each mouse were placed in individually labeled tubes, fixed in 4% buffered formalin, paraffin embedded, and sectioned. The histological score was assessed using H&E stained sections. Joints were scored for inflammation, cartilage damage, pannus formation, and bone resorption on a scale of 0 to 3 for each readout. Two-way ANOVA statistical analysis was performed.

#### 4.19. Docking

Prior to docking, the protein (PECAM-1 IgL1-2 trans-homophilic dimer, PDB code: 5GNI) was prepared using the prepared protein protocol, as implemented in Maestro (Schrödinger, USA) to assign the correct protonation states to titrate-able residues. The structures of the active (**12**, **26**, **4**, **11**, **13**, **23**, and **24**) and inactive compounds (**1**, **2**, **3**, **14**, and **22**) were processed by Ligprep as implemented in Maestro, to assign correct protonation states at a physiological pH. Prior to docking, potential druggable binding sites in PECAM-1 were identified using SiteMap. Five possible binding sites were identified (Fig. 14A). Grid boxes were centered on the identified sites. Docking of all compounds to all sites was performed using the induced fit docking (IFD) protocol in which residues within 10 Å of any of the resulting top 20 ligand poses (from the initial docking) were subjected to a conformational search and minimization, whereas residues outside the region were kept fixed [81–83]. The IFD score consists of GlideScore SP + 0.05 × PrimeEnergy [83]. The resulting poses from the docking procedure were sorted by the IFD score and subjected to enrichment calculation, as implemented in Maestro to produce ROC curves. These plots were used to rank the different binding sites in terms of their ability to distinguish between active and inactive compounds.

#### 4.20. PK study

Twelve C57 black mice received compound **12**, PO (gavage, 50 mg/kg) in DMSO 70 µL per mice. Three mice received only DMSO and were used as a control for zero time point. At time 30 min, 2.5 h, 6 h and 9 h, three mice per time point were euthanized and whole blood was taken from heart aspiration. The blood was centrifuged for 2000 rpm/10 min. Plasma was treated by acetonitrile (70 µL per y 200 µL of plasma) and extracted by chloroform (4 mL per 1 mL of plasma). Chloroform was transferred to a clean tube and evaporated until dryness. The obtained residue was dissolved in 100 µL of DMSO and injected to LC-MS. Spiking and calibration curve were generated using plasma of the non-treated mice.

## 5. Patent

All data described in the manuscript are protected by patent appl. No. 62/552,491.

## Author contributions

The manuscript was written through the contributions of all authors. T.G., R.M., P.B., E.A., R. L., B.I., H.S., and A.G., designed the experiments. T.G., R.M., E.A., P.B., S.Z., N.K., N. K-L., S.K., E.B., N.H. and L.L. performed the experiments. All authors have approved the final version of the manuscript.

## Acknowledgements

This study was supported by a Bar-Ilan University new faculty grant (to A.G). T.G was the recipient of a Lev Zion Fellowship, Israel. S.K. is grateful for the support of her work by the Wolf Foundation, Israel. We thank Mr. Steven Manch for the English editing.

## Appendix A. Supplementary material

Supplementary data to this article can be found online at <https://doi.org/10.1016/j.bioorg.2019.103250>.

## References

- [1] A. Watad, S. Azrielant, N.L. Bragazzi, K. Sharif, P. David, I. Katz, G. Aljadef, M. Quaresma, G. Tanay, M. Adawi, H. Amital, Y. Shoenfeld, Seasonality and auto-immune diseases: The contribution of the four seasons to the mosaic of auto-immunity, *J. Autoimmun.* 82 (2017) 13–30.
- [2] L. Wang, F.S. Wang, M.E. Gershwin, Human autoimmune diseases: a comprehensive update, *J. Intern. Med.* 278 (4) (2015) 369–395.
- [3] E. Kalaitzoglou, I. Popescu, R.C. Bunn, J.L. Fowlkes, K.M. Thraillkill, Effects of type 1 diabetes on osteoblasts, osteocytes, and osteoclasts, *Curr. Osteoporos. Rep.* 14 (6) (2016) 310–319.
- [4] G. Azizi, H. Abolhassani, M.H. Asgardoone, T. Alinia, R. Yazdani, J. Mohammadi, N. Rezaei, H.D. Ochs, A. Aghamohammadi, Autoimmunity in common variable immunodeficiency: epidemiology, pathophysiology and management, *Expert Rev. Clin. Immunol.* 13 (2) (2017) 101–115.
- [5] M.D. Rosenblum, L.K. Gratz, J.S. Paw, A.K. Abbas, Treating human autoimmunity: current practice and future prospects, *Sci. Transl. Med.* 4 (125) (2012) 125sr1.
- [6] A. Sala, E. Proschak, D. Steinhilber, G.E. Rovati, Two-pronged approach to anti-inflammatory therapy through the modulation of the arachidonic acid cascade, *Biochem. Pharmacol.* 158 (2018) 161–173.
- [7] M. Del Grossi Moura, L. Cruz Lopes, M.T. Silva, S. Barberato-Filho, R.H.L. Motta, C.C. Bergamaschi, Use of steroid and nonsteroidal anti-inflammatories in the treatment of rheumatoid arthritis: Systematic review protocol, *Medicine (Baltimore)* 97 (41) (2018) e12658.
- [8] J. Saad, M.V. Pellegrini, Nonsteroidal anti-inflammatory drugs (NSAID) toxicity, *StatPearls, Treasure Island (FL)*, (2018).
- [9] C.C. Chow, S.S. Simons Jr., An approach to greater specificity for glucocorticoids, *Front. Endocrinol. (Lausanne)* 9 (2018) 76.
- [10] M. Jastrzebska, M.E. Czok, P. Guzik, Autoimmune diseases, their pharmacological treatment and the cardiovascular system, *Cardiol. J.* 20 (6) (2013) 569–576.
- [11] S.L. Thomas, C. Griffiths, L. Smeeth, C. Rooney, A.J. Hall, Burden of mortality associated with autoimmune diseases among females in the United Kingdom, *Am. J. Public Health* 100 (11) (2010) 2279–2287.
- [12] G.S. Hamilton, R.E. Mewshaw, C.M. Bryant, Y. Feng, G. Endemann, K.S. Madden, J.E. Janczak, J. Perumattam, L.W. Stanton, X. Yang, et al., Fluorenylalkanoic and benzoic acids as novel inhibitors of cell adhesion processes in leukocytes, *J. Med. Chem.* 38 (10) (1995) 1650–1656.
- [13] F.A. Acker, H.P. Voss, H. Timmerman, Chemokines: structure, receptors and functions. A new target for inflammation and asthma therapy? *Mediators Inflamm* 5 (6) (1996) 393–416.
- [14] K. Ley, J. Rivera-Nieves, W.J. Sandborn, S. Shattil, Integrin-based therapeutics: biological basis, clinical use and new drugs, *Nat. Rev. Drug Discov.* 15 (3) (2016) 173–183.
- [15] P. Vanderslice, D.G. Woodside, Integrin antagonists as therapeutics for inflammatory diseases, *Expert Opin. Invest. Drugs* 15 (10) (2006) 1235–1255.
- [16] S.L. Goodman, M. Picard, Integrins as therapeutic targets, *Trends Pharmacol. Sci.* 33 (7) (2012) 405–412.
- [17] M.J. Briskin, L.M. McEvoy, E.C. Butcher, MAdCAM-1 has homology to immunoglobulin and mucin-like adhesion receptors and to IgA1, *Nature* 363 (6428) (1993) 461–464.
- [18] E.E. Sikorski, R. Hallmann, E.L. Berg, E.C. Butcher, The Peyer's patch high endothelial receptor for lymphocytes, the mucosal vascular addressin, is induced on a murine endothelial cell line by tumor necrosis factor- $\alpha$  and IL-1, *J. Immunol.* 151 (10) (1993) 5239–5250.
- [19] R.K. Pachynski, S.W. Wu, M.D. Gunn, D.J. Erle, Secondary lymphoid-tissue chemokine (SLC) stimulates integrin  $\alpha$ 4  $\beta$ 7-mediated adhesion of lymphocytes to mucosal addressin cell adhesion molecule-1 (MAdCAM-1) under flow, *J. Immunol.* 161 (2) (1998) 952–956.
- [20] S. Thomas, D.C. Baumgart, Targeting leukocyte migration and adhesion in Crohn's disease and ulcerative colitis, *Inflammopharmacology* 20 (1) (2012) 1–18.
- [21] H. Hoshino, M. Kobayashi, J. Mitoma, Y. Sato, M. Fukuda, J. Nakayama, An integrin  $\alpha$ 4 $\beta$ 7\* $\beta$ 7 IgG heterodimeric chimera binds to MAdCAM-1 on high endothelial venules in gut-associated lymphoid tissue, *J. Histochem. Cytochem.* 59 (6) (2011) 572–583.
- [22] T. Ando, R.R. Langley, Y. Wang, P.A. Jordan, A. Minagar, J.S. Alexander, M.H. Jennings, Inflammatory cytokines induce MAdCAM-1 in murine hepatic endothelial cells and mediate  $\alpha$ 4  $\beta$ 7 integrin dependent lymphocyte endothelial adhesion in vitro, *BMC Physiol.* 7 (2007) 10.
- [23] E.J. Park, J.R. Mora, C.V. Carman, J. Chen, Y. Sasaki, G. Cheng, U.H. von Andrian, M. Shimaoka, Aberrant activation of integrin  $\alpha$ 4 $\beta$ 7 suppresses lymphocyte migration to the gut, *J. Clin. Invest.* 117 (9) (2007) 2526–2538.
- [24] S. Ghosh, R. Panaccione, Anti-adhesion molecule therapy for inflammatory bowel disease, *Therap. Adv. Gastroenterol.* 3 (4) (2010) 239–258.
- [25] S. Vermeire, W.J. Sandborn, S. Danese, X. Hebuterne, B.A. Salzberg, M. Klopocka, D. Tarabar, T. Vanasek, M. Gregus, P.A. Hellstern, J.S. Kim, M.P. Sparrow, K.J. Gorelick, M. Hinz, A. Ahmad, V. Pradhan, M. Hassan-Zahraee, R. Clare, F. Cataldi, W. Reinisch, Anti-MAdCAM antibody (PF-00547659) for ulcerative colitis (TURANDOT): a phase 2, randomised, double-blind, placebo-controlled trial, *Lancet* 390 (10090) (2017) 135–144.
- [26] M.L. Scribano, Vedolizumab for inflammatory bowel disease: From randomized controlled trials to real-life evidence, *World J. Gastroenterol.* 24 (23) (2018) 2457–2467.
- [27] J.L. Viney, S. Jones, H.H. Chiu, B. Lagrimas, M.E. Renz, L.G. Presta, D. Jackson, K.J. Hillan, S. Lew, S. Fong, Mucosal addressin cell adhesion molecule-1: a structural and functional analysis demarcates the integrin binding motif, *J. Immunol.* 157 (6) (1996) 2488–2497.
- [28] H.N. Shroff, C.F. Schwender, A.D. Baxter, F. Brookfield, L.J. Payne, N.A. Cochran, D.L. Gallant, M.J. Briskin, Novel modified tripeptide inhibitors of  $\alpha$ 4  $\beta$ 7 mediated lymphoid cell adhesion to MAdCAM-1, *Bioorg. Med. Chem. Lett.* 8 (13) (1998) 1601–1606.
- [29] J. Boer, D. Gottschling, A. Schuster, M. Semmrich, B. Holzmann, H. Kessler, Design and synthesis of potent and selective  $\alpha$ (4) $\beta$ (7) integrin antagonists, *J. Med. Chem.* 44 (16) (2001) 2586–2592.
- [30] N.J. Dubree, D.R. Artis, G. Castanedo, J. Marsters, D. Sutherlin, L. Caris, K. Clark, S.M. Keating, M.H. Beresini, H. Chiu, S. Fong, H.B. Lowman, N.J. Skelton, D.Y. Jackson, Selective  $\alpha$ 4 $\beta$ 7 integrin antagonists and their potential as antiinflammatory agents, *J. Med. Chem.* 45 (16) (2002) 3451–3457.
- [31] G.M. Castanedo, F.C. Sailes, N.J. Dubree, J.B. Nicholas, L. Caris, K. Clark, S.M. Keating, M.H. Beresini, H. Chiu, S. Fong, J.C. Marsters Jr., D.Y. Jackson, D.P. Sutherlin, Solid-phase synthesis of dual  $\alpha$ 4 $\beta$ 7 integrin antagonists: two scaffolds with overlapping pharmacophores, *Bioorg. Med. Chem. Lett.* 12 (20) (2002) 2913–2917.
- [32] A.B. Dyatkin, Y. Gong, T.A. Miskowski, E.S. Kimball, S.M. Prouty, M.C. Fisher, R.J. Santulli, C.R. Schneider, N.H. Wallace, P.J. Hornby, C. Diamond, W.A. Kinney, B.E. Maryanoff, B.P. Damiano, W. He, Aza-bicyclic amino acid carboxamides as  $\alpha$ 4 $\beta$ 7 integrin receptor antagonists, *Bioorg. Med. Chem.* 13 (24) (2005) 6693–6702.
- [33] G.C. Harriman, M. Brewer, R. Bennett, C. Kuhn, M. Bazin, G. Larosa, P. Skerker, N. Cochran, D. Gallant, D. Baxter, D. Picarella, B. Jaffee, J.R. Luly, M.J. Briskin, Selective cell adhesion inhibitors: Barbituric acid based  $\alpha$ 4 $\beta$ 7–MAdCAM inhibitors, *Bioorg. Med. Chem. Lett.* 18 (7) (2008) 2509–2512.
- [34] C. Xu, A.R. Wyman, M.A. Alaamery, S.A. Argueta, F.D. Ivey, J.A. Meyers, A. Lerner, T.H. Burdo, T. Connolly, C.S. Hoffman, T.C. Chiles, Anti-inflammatory effects of novel barbituric acid derivatives in T lymphocytes, *Int. Immunopharmacol.* 38 (2016) 223–232.
- [35] V. Temml, T. Kaserer, Z. Kutil, P. Landa, T. Vanek, D. Schuster, Pharmacophore modeling for COX-1 and -2 inhibitors with LigandScout in comparison to Discovery Studio, *Future Med. Chem.* 6 (17) (2014) 1869–1881.
- [36] G. Wolber, T. Langer, LigandScout: 3-D pharmacophores derived from protein-bound ligands and their use as virtual screening filters, *J. Chem. Inf. Model.* 45 (1) (2005) 160–169.
- [37] J.D. Figueroa-Villar, A.A. Vieira, Nuclear magnetic resonance and molecular modeling study of exocyclic carbon-carbon double bond polarization in benzylidene barbiturates, *J. Mol. Struct.* 1034 (2013) 310–317.
- [38] E. Knoevenagel, Condensation von Malonsäure mit aromatischen Aldehyden durch Ammoniak und Amine, *Ber. Dtsch. Chem. Ges.* 31 (3) (1898) 2596–2619.
- [39] K.M. Khan, M. Ali, M. Khan, M. Taha, S. Perveen, NH<sub>4</sub>Cl mediated new protocol for the synthesis of 5-arylidene barbiturates, *Lett. Org. Chem.* 8 (1) (2011) 28–32.
- [40] J. Lasri, G. Gajewski, M.F.C.G. da Silva, M.L. Kuznetsov, R.R. Fernandes, A.J.L. Pombreiro, Solvent-dependent reactivities of acyclic nitrones with beta-diketones: catalyst-free syntheses of endiones and enones, *Tetrahedron* 68 (35) (2012) 7019–7027.
- [41] S. Vassiliou, M. Xeilari, A. Yiotakis, J. Grembecka, M. Pawelczak, P. Kafarski, A. Mucha, A synthetic method for diversification of the P1' substituent in phosphonic dipeptides as a tool for exploration of the specificity of the S1' binding pockets of leucine aminopeptidases, *Bioorg. Med. Chem.* 15 (9) (2007) 3187–3200.
- [42] N. Zidar, T. Tomasic, R. Sink, A. Kovac, D. Patin, D. Blanut, C. Contreras-Martel, A. Dessen, M.M. Premru, A. Zega, S. Gobec, L.P. Masic, D. Kikelj, New 5-benzylidene-thiazolidin-4-one inhibitors of bacterial MurD ligase: design, synthesis, crystal structures, and biological evaluation, *Eur. J. Med. Chem.* 46 (11) (2011) 5512–5523.
- [43] E.C. Butcher, Leukocyte-endothelial cell recognition: three (or more) steps to specificity and diversity, *Cell* 67 (6) (1991) 1033–1036.
- [44] P.F. Bradford, C. Scheiermann, S. Nourshargh, C. Ody, F.W. Lusinskas, G.E. Rainger, G.B. Nash, M. Miljkovic-Licina, M. Aurrand-Lions, B.A. Imhof, JAM-C

- regulates unidirectional monocyte transendothelial migration in inflammation, *Blood* 110 (7) (2007) 2545–2555.
- [45] H.S. Schultz, S.L. Reedtz-Runge, B.T. Backstrom, K. Lamberth, C.R. Pedersen, A.M. Kvarnhammar, A. Consortium, Quantitative analysis of the CD4+ T cell response to therapeutic antibodies in healthy donors using a novel T cell: PBMC assay, *PLoS One* 12 (5) (2017) e0178544.
- [46] A. Mathias, S. Perriot, M. Canales, C. Blatti, C. Gaubicher, M. Schlupe, B. Engelhardt, R. Du Pasquier, Impaired T-cell migration to the CNS under fingolimod and dimethyl fumarate, *Neurol. Neuroimmunol. Neuroinflamm.* 4 (6) (2017) e401.
- [47] M.K. Racke, Y. Yang, A.E. Lovett-Racke, Is T-bet a potential therapeutic target in multiple sclerosis? *J. Interferon Cytokine Res.* 34 (8) (2014) 623–632.
- [48] C. Zanotti, M. Chiarini, F. Serana, A. Sottini, E. Garrafa, F. Torri, L. Caimi, S. Rasia, R. Capra, L. Imberti, Peripheral accumulation of newly produced T and B lymphocytes in natalizumab-treated multiple sclerosis patients, *Clin. Immunol.* 145 (1) (2012) 19–26.
- [49] S.K. Alford, G.D. Longmore, W.F. Stenson, C. Kemper, CD46-induced immunomodulatory CD4+ T cells express the adhesion molecule and chemokine receptor pattern of intestinal T cells, *J. Immunol.* 181 (4) (2008) 2544–2555.
- [50] T.T. Ho, J.O. You, D.T. Auguste, siRNA Delivery Impedes the Temporal Expression of Cytokine-Activated VCAM1 on Endothelial Cells, *Ann. Biomed. Eng.* 44 (4) (2016) 895–902.
- [51] C. Donate, C. Ody, T. McKee, S. Ruault-Jungblut, N. Fischer, P. Ropraz, B.A. Imhof, T. Matthes, Homing of human B cells to lymphoid organs and B-cell lymphoma engraftment are controlled by cell adhesion molecule JAM-C, *Cancer Res.* 73 (2) (2013) 640–651.
- [52] T.L. Rogers, D. Wallick, Reviewing the use of ethylcellulose, methylcellulose and hypromellose in microencapsulation. Part 1: materials used to formulate microcapsules, *Drug Dev. Ind. Pharm.* 38 (2) (2012) 129–157.
- [53] Y.H. Li, H.T. Xiao, D.D. Hu, S. Fatima, C.Y. Lin, H.X. Mu, N.P. Lee, Z.X. Bian, Berberine ameliorates chronic relapsing dextran sulfate sodium-induced colitis in C57BL/6 mice by suppressing Th17 responses, *Pharmacol. Res.* 110 (2016) 227–239.
- [54] Y.H. Park, N. Kim, Y.K. Shim, Y.J. Choi, R.H. Nam, Y.J. Choi, M.H. Ham, J.H. Suh, S.M. Lee, C.M. Lee, H. Yoon, H.S. Lee, D.H. Lee, Adequate dextran sodium sulfate-induced colitis model in mice and effective outcome measurement method, *J. Cancer Prev.* 20 (4) (2015) 260–267.
- [55] C.S. Moore, A.L. Hebb, M.M. Blanchard, C.E. Crocker, P. Liston, R.G. Korneluk, G.S. Robertson, Increased X-linked inhibitor of apoptosis protein (XIAP) expression exacerbates experimental autoimmune encephalomyelitis (EAE), *J. Neuroimmunol.* 203 (1) (2008) 79–93.
- [56] L. Ma, S. Li, H. Zheng, J. Chen, L. Lin, X. Ye, Z. Chen, Q. Xu, T. Chen, J. Yang, N. Qiu, G. Wang, A. Peng, Y. Ding, Y. Wei, L. Chen, Synthesis and biological activity of novel barbituric and thiobarbituric acid derivatives against non-alcoholic fatty liver disease, *Eur. J. Med. Chem.* 46 (6) (2011) 2003–2010.
- [57] L. Ma, C. Xie, Y. Ran, X. Liang, L. Huang, H. Pei, J. Chen, J. Liu, Y. Sang, H. Lai, A. Peng, M. Xiang, Y. Wei, L. Chen, Synthesis and biological evaluation of 5-benzylidene-pyrimidine-2,4,6-(1H,3H,5H)-trione derivatives for the treatment of obesity-related nonalcoholic fatty liver disease, *J. Med. Chem.* 55 (22) (2012) 9958–9972.
- [58] H. Zheng, S. Li, L. Ma, L. Cheng, C. Deng, Z. Chen, C. Xie, M. Xiang, W. Jiang, L. Chen, A novel agonist of PPAR-gamma based on barbituric acid alleviates the development of non-alcoholic fatty liver disease by regulating adipocytokine expression and preventing insulin resistance, *Eur. J. Pharmacol.* 659 (2–3) (2011) 244–251.
- [59] T. Kanazawa, K. Tamano, K. Sogabe, T. Endo, H. Ibaraki, Y. Takashima, Y. Seta, Intra-articular retention and anti-arthritis effects in collagen-induced arthritis model mice by injectable small interfering RNA containing hydrogel, *Biol. Pharm. Bull.* 40 (11) (2017) 1929–1933.
- [60] H. DeLisser, Y. Liu, P.Y. Desprez, A. Thor, P. Briassoulis, C. Handumrongkul, J. Wilfong, G. Yount, M. Nosrati, S. Fong, E. Shtivelman, M. Fehrenbach, G. Cao, D.H. Moore, S. Nayak, D. Liggitt, M. Kashani-Sabet, R. Debs, Vascular endothelial platelet endothelial cell adhesion molecule 1 (PECAM-1) regulates advanced metastatic progression, *Proc. Natl. Acad. Sci. USA* 107 (43) (2010) 18616–18621.
- [61] Z. Qing, M. Sandor, Z. Radvany, D. Sewell, A. Falus, D. Potthoff, W.A. Muller, Z. Fabry, Inhibition of antigen-specific T cell trafficking into the central nervous system via blocking PECAM1/CD31 molecule, *J. Neuropathol. Exp. Neurol.* 60 (8) (2001) 798–807.
- [62] Z. Mamdouh, G.E. Kreitzer, W.A. Muller, Leukocyte transmigration requires kinesin-mediated microtubule-dependent membrane trafficking from the lateral border recycling compartment, *J. Exp. Med.* 205 (4) (2008) 951–966.
- [63] C. Paddock, D. Zhou, P. Lertkiatmongkol, P.J. Newman, J. Zhu, Structural basis for PECAM-1 homophilic binding, *Blood* 127 (8) (2016) 1052–1061.
- [64] K. Hashimoto, N. Kataoka, E. Nakamura, K. Hagihara, M. Hatano, T. Okamoto, H. Kanouchi, Y. Minatogawa, S. Mohri, K. Tsujioka, F. Kajiya, Monocyte trans-endothelial migration augments subsequent transmigration activity with increased PECAM-1 and decreased VE-cadherin at endothelial junctions, *Int. J. Cardiol.* 149 (2) (2011) 232–239.
- [65] K. Hashimoto, N. Kataoka, E. Nakamura, K. Tsujioka, F. Kajiya, Oxidized LDL specifically promotes the initiation of monocyte invasion during transendothelial migration with upregulated PECAM-1 and downregulated VE-cadherin on endothelial junctions, *Atherosclerosis* 194 (2) (2007) e9–e17.
- [66] D. Bartusik, B. Tomanek, Detection of (19)F-labeled biopharmaceuticals in cell cultures with magnetic resonance, *Adv. Drug Deliv. Rev.* 65 (8) (2013) 1056–1064.
- [67] M. Srinivas, P. Boehm-Sturm, C.G. Figdor, I.J. de Vries, M. Hoehn, Labeling cells for in vivo tracking using (19)F MRI, *Biomaterials* 33 (34) (2012) 8830–8840.
- [68] B. Gaye, A. Adejare, Fluorinated molecules in the diagnosis and treatment of neurodegenerative diseases, *Future Med. Chem.* 1 (5) (2009) 821–833.
- [69] S. Xu, X. Du, G. Feng, Y. Zhang, J. Li, B. Lin, L. Yang, S. Fu, J. Wu, Efficient inhibition of cervical cancer by dual drugs loaded in biodegradable thermosensitive hydrogel composites, *Oncotarget* 9 (1) (2018) 282–292.
- [70] B. Klemetsen, L. Jorgensen, Distribution of adhesion molecules on HeLa cells, platelets and endothelium in an in vitro model mimicking the early phase of metastasis An immunogold electron microscopic study, *APMIS* 105 (7) (1997) 546–558.
- [71] S. Muro, V.R. Muzykantor, Targeting of antioxidant and anti-thrombotic drugs to endothelial cell adhesion molecules, *Curr. Pharm. Des.* 11 (18) (2005) 2383–2401.
- [72] B.S. Ding, C. Gottstein, A. Grunow, A. Kuo, K. Ganguly, S.M. Albelda, D.B. Cines, V.R. Muzykantor, Endothelial targeting of a recombinant construct fusing a PECAM-1 single-chain variable antibody fragment (scFv) with prourokinase facilitates prophylactic thrombolysis in the pulmonary vasculature, *Blood* 106 (13) (2005) 4191–4198.
- [73] S. Muro, C. Gajewski, M. Koval, V.R. Muzykantor, ICAM-1 recycling in endothelial cells: a novel pathway for sustained intracellular delivery and prolonged effects of drugs, *Blood* 105 (2) (2005) 650–658.
- [74] C. Garnacho, S.M. Albelda, V.R. Muzykantor, S. Muro, Differential intra-endothelial delivery of polymer nanocarriers targeted to distinct PECAM-1 epitopes, *J. Control. Release* 130 (3) (2008) 226–233.
- [75] P.F. Bradfield, A. Menon, M. Miljkovic-Licina, B.P. Lee, N. Fischer, R.J. Fish, B. Kwak, E.A. Fisher, B.A. Imhof, Divergent JAM-C expression accelerates monocyte-derived cell exit from atherosclerotic plaques, *PLoS ONE* 11 (7) (2016) e0159679.
- [76] W. He, S. Holtkamp, S.M. Hergenhan, K. Kraus, A. de Juan, J. Weber, P. Bradfield, J.M.P. Grenier, J. Pelletier, D. Druzdz, C.S. Chen, L.M. Ince, S. Bierschenk, R. Pick, M. Sperandio, M. Aurrand-Lions, C. Scheiermann, Circadian expression of migratory factors establishes lineage-specific signatures that guide the homing of leukocyte subsets to tissues, *Immunity* 49 (6) (2018) pp. 1175–1190 e7.
- [77] A. Sidibe, P. Ropraz, S. Jemelin, Y. Emre, M. Poittevin, M. Pocard, P.F. Bradfield, B.A. Imhof, Angiogenic factor-driven inflammation promotes extravasation of human proangiogenic monocytes to tumours, *Nat. Commun.* 9 (1) (2018) 355.
- [78] P. Ropraz, B.A. Imhof, T. Matthes, B. Wehrle-Haller, A. Sidibe, Simultaneous study of the recruitment of monocyte subpopulations under flow in vitro, *J. Vis. Exp.* (141) (2018).
- [79] O. Ozgun-Acar, G. Celik-Turgut, I. Gazioglu, U. Kolak, S. Ozbil, B.U. Ergur, S. Arslan, A. Sen, G. Topcu, Capparis ovata treatment suppresses inflammatory cytokine expression and ameliorates experimental allergic encephalomyelitis model of multiple sclerosis in C57BL/6 mice, *J. Neuroimmunol.* 298 (2016) 106–116.
- [80] A. Hoehne, M.L. James, I.S. Alam, J.A. Ronald, B. Schneider, A. D'Souza, T.H. Witney, L.E. Andrews, H.C. Cropper, D. Behera, G. Gowrishankar, Z. Ding, T. Wyss-Coray, F.T. Chin, S. Biswal, S.S. Gambhir, [(18)F]FSPG-PET reveals increased cystine/glutamate antiporter (xc-) activity in a mouse model of multiple sclerosis, *J. Neuroinflammation* 15 (1) (2018) 55.
- [81] T.A. Halgren, Identifying and characterizing binding sites and assessing drugability, *J. Chem. Inf. Model.* 49 (2) (2009) 377–389.
- [82] R. Farid, T. Day, R.A. Friesner, R.A. Pearlstein, New insights about HERG blockade obtained from protein modeling, potential energy mapping, and docking studies, *Bioorg. Med. Chem.* 14 (9) (2006) 3160–3173.
- [83] W. Sherman, T. Day, M.P. Jacobson, R.A. Friesner, R. Farid, Novel procedure for modeling ligand/receptor induced fit effects, *J. Med. Chem.* 49 (2) (2006) 534–553.